Earth's Future

RESEARCH ARTICLE
10.1029/2024EF004996

Key Points:

- Most newly thawed permafrost C would be retained in deep layers in the 21st century
- Permafrost degradation would reduce ecosystem C stocks
- Climate change, CO_2 fertilization, and permafrost degradation collectively affect ecosystem C cycling

Supporting Information:

Supporting Information may be found in the online version of this article.

Correspondence to:

D. Zhao,
zhaods@igsnrr.ac.cn

Citation:

Liu, L., Zhuang, Q., Zhao, D., Wei, J., & Zheng, D. (2024). The fate of deep permafrost carbon in northern high latitudes in the 21st century: A process-based modeling analysis. *Earth's Future*, *12*, e2024EF004996. https://doi.org/10.1029/2024EF004996

Received 9 JUN 2024
Accepted 11 OCT 2024

Author Contributions:

Conceptualization: L. Liu, Q. Zhuang
Formal analysis: L. Liu
Investigation: L. Liu
Methodology: J. Wei, D. Zheng
Supervision: Q. Zhuang, D. Zheng
Visualization: L. Liu
Writing – original draft: L. Liu
Writing – review & editing: L. Liu, Q. Zhuang, J. Wei, D. Zheng

The Fate of Deep Permafrost Carbon in Northern High Latitudes in the 21st Century: A Process-Based Modeling Analysis

L. Liu[1,2,3], Q. Zhuang[3], D. Zhao[2], J. Wei[4], and D. Zheng[2]

[1]The School of Geo-Science and Technology, Zhengzhou University, Zhengzhou, China, [2]Key Laboratory of Land Surface Pattern and Simulation, Institute of Geographic Sciences and Natural Resources Research, Chinese Academy of Sciences, Beijing, China, [3]Department of Earth, Atmospheric, and Planetary Sciences, Purdue University, West Lafayette, IN, USA, [4]School of Urban and Rural Planning, Henan University of Economics and Law, Zhengzhou, China

Abstract Warming in permafrost regions stimulates carbon (C) release through decomposition, but increasing atmospheric CO_2 and available soil nitrogen enhance plant productivity at the same time. To date, a large uncertainty in the regional C dynamics still remains. Here we use a process-based biogeochemical model by considering C exposure from thawed permafrost and observational data to quantify permafrost C emissions and ecosystem C budget in northern high latitudes in the 21st century. Permafrost degradation will make 119.3 Pg and 251.6 Pg C available for decomposition by 2100 under the Shared Socioeconomic Pathway (SSP)126 and SSP585, respectively. However, only 4–8% of the newly thawed permafrost C is expected to be released into the atmosphere by 2100. Cumulatively, permafrost degradation will reduce ecosystem C stocks by 3.37 Pg and 15.37 Pg under the SSP126 and SSP585, respectively. Additionally, CO_2 fertilization effects would stimulate plant productivity and increase ecosystem C stocks substantially. The combined effects of climate change, CO_2 fertilization, and permafrost degradation on C fluxes are typically more profound than any single factor, emphasizing the intricate interplay between these elements in shaping permafrost C-climate feedbacks. Our study suggests that the majority of the thawed C will remain sequestered in previously frozen layers in this century, posing a significant challenge to climate change mitigation efforts once any process accelerates the decomposition of this huge amount of thawed C.

Plain Language Summary Amplified warming in permafrost areas accelerates permafrost degradation, thereby exposing vast quantities of previously frozen carbon (C) that has the potential to strongly feedback to global climate upon decomposition. Nevertheless, the amount of C that would be released into the atmosphere as a result of permafrost thawing remains uncertain. To refine our predictions of permafrost C loss, we leveraged observational data to constrain C exposure from thawed permafrost and simulated its decomposition by accounting for varying soil conditions at different depths. Our findings indicate that 119.3 and 251.6 billion tons of previously frozen C would be subject to microbial decomposition by 2100 under the Shared Socioeconomic Pathway (SSP) 1–2.6 and SSP 5–8.5, respectively. However, the majority of this newly thawed C is likely to remain sequestered in deep soil layers this century, with only a minor fraction (4%–8%) decomposing and releasing into the atmosphere. A potential mitigating factor is the enhanced plant C assimilation due to rising atmospheric CO_2 concentrations. Our research underscores the significant threat that the substantial amount of newly thawed C poses to climate change mitigation efforts, particularly if any process accelerates the decomposition of organic C in deep soil layers.

1. Introduction

Permafrost soil contains large amounts of organic carbon (1,014 Pg for 0–3 m depth; Mishra et al., 2021) that is vulnerable to climate warming and may accelerate climate change through greenhouse gas emission (Schuur et al., 2015, 2022). Despite the potential strong positive feedback from permafrost carbon (C) to global climate, substantial uncertainties remain in the projections of the locations, timing, and magnitudes of permafrost C release (McGuire et al., 2018; Miner et al., 2022). These uncertainties could result from (a) the harsh, wide, and remote environment that is not well represented in observations (Gay et al., 2023; Mishra et al., 2021; Palmtag et al., 2022); (b) the complex and unique water, energy, carbon, and nutrient interactions among the atmosphere, plants, soils, frozen layers, and microbes (Ramm et al., 2022; Schuur et al., 2022; Virkkala et al., 2021); and (c) the far-reaching impacts caused by unpredictable weather extremes (e.g., drought and flooding), disturbances (e.g., abrupt thaw and wildfires), and their interactions (Foster et al., 2022; Meredith et al., 2019; Treat et al., 2024).

Process models represent a state-of-the-art understanding of processes at various scales and are critical tools for evaluating permafrost C-climate feedback. Over the years, process models have made important advances in their land surface schemes, like accounting for changes in the thermal and hydraulic properties due to soil freezing (Yokohata et al., 2020), and representing the insulating effects of snow, moss, and peat soils (Stepanenko et al., 2020; Tao et al., 2024). However, large uncertainties remain in projections of future permafrost C budget (Natali et al., 2022), for example, the maximum standard deviation of annual terrestrial net ecosystem exchange for the process models in Inter-Sectoral Impact Model Intercomparison Project (ISIMIP) can be as large as 104 g C m^{-2} y^{-1} (Treat et al., 2024). Inaccurate representations of vegetation coverages and soil C stocks (Varney et al., 2022) and the missing of important processes such as vegetation dynamics, nitrogen limitations, and disturbances-permafrost-carbon interactions (Canadell et al., 2021; Miner et al., 2022; Turetsky et al., 2020) all contribute to the large model discrepancies. Most importantly, most earth system models (ESMs) in Coupled Model Intercomparison Phase 6 (CMIP6) assessed for the IPCC AR6 report did not represent permafrost C at all (Schädel et al., 2024).

One crucial characteristic of permafrost C is that long-term storage can occur in deep soils. Although soil organic C (SOC) stocks are consistently greater at 0–1 m than in deeper intervals (Mishra et al., 2021), substantial permafrost C exists below 3-m depth, particularly for Yedoma deposits and Arctic river deltas (Schuur et al., 2022). It has been found that permafrost C-climate feedback is sensitive to C decomposability in deep soils (Koven et al., 2015). However, many permafrost models usually simulate soil C dynamics (like litter turnover, SOC accumulation and decomposition) in around top 3 m (McGuire et al., 2016). Moreover, the initial stocks of permafrost C in these models are normally decided during model spin-up, using pre-industrial climate until the soil carbon is relatively stable between spin-up iterations. Because many relevant processes such as alluvial sedimentation, peat development and cryoturbation are often missed in permafrost models (Ping et al., 2015; Schuur et al., 2008), there can be biases in soil carbon stocks (Foereid et al., 2012). Burke et al. (2017) found that simulated deep soil C storage (251 Pg) below 1 m through spin-up can be half of the observation (585 Pg) for permafrost regions. Consequently, the amount of thawed C calculated based on the initial C stocks may deviate from reality, reducing the accuracy of projected permafrost C emission. However, observational data on permafrost C content along soil profile have been accumulating over the years (Ding et al., 2016; Hugelius et al., 2014; Mishra et al., 2021; Wang et al., 2020). By combining these soil C profile data with land surface models that consider soil C exposure with thawing depth, model studies shall make a more accurate estimation of thawed C amount, more reliable permafrost C emissions, and better-constrained net carbon balance in northern high latitudes.

This study revised a process-based biogeochemical model to incorporate soil C exposure and decomposition due to permafrost thaw in deep soils (up to six m), and integrated observational-based data sets of SOC profiles along soil depth into the model to improve the quantification accuracy of permafrost C exposure. Based on the modified model, a simulation protocol was used to quantify (a) the amount of newly-thawed permafrost C in the 21st century and the C release into the atmosphere due to permafrost thaw, (b) the net effects of permafrost degradation on ecosystem C balance, and (c) the interactions between permafrost degradation and other climate change factors concerning their relative importance in permafrost C emission.

2. Materials and Methods

2.1. The Terrestrial Ecosystem Model

The Terrestrial Ecosystem Model (TEM) is a process-based biogeochemistry model that uses spatially referenced information on climate, elevation, soils, vegetation, and soil- and vegetation-specific parameters to estimate C and N fluxes and pool sizes of terrestrial ecosystems (Raich et al., 1991). TEM models C and N cycling processes and the regulations of environmental factors on those processes. Important feedback and constraints on C and N fluxes and pools are considered in TEM. TEM is directly linked to a water balance model and a soil thermal model; therefore, interactions between C and N cycling, soil temperature, and moisture availability are explicitly treated. The coupling of C and N cycling also enables TEM to consider the constraints of N availability on C uptake (McGuire et al., 1993). Detailed descriptions of TEM have been documented in previous works (McGuire et al., 1992, 1993; Raich et al., 1991; Zhuang et al., 2001, 2011). A brief description of the soil thermal model that

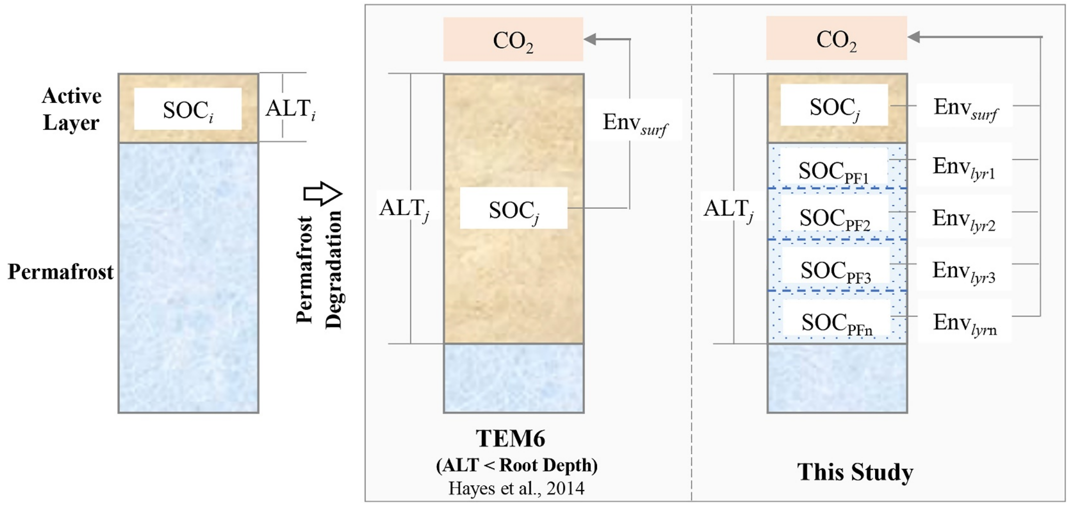

Figure 1. The modification of Terrestrial Ecosystem Model (TEM) to represent permafrost carbon with depth. i and j are timestamps before and after permafrost degradation, respectively. TEM6 treats all the SOC in the active layer as a whole, and its decomposition is affected by soil temperature and moisture of the surface (top 20 cm) layer (Env$_{surf}$). SOC below rooting depth is excluded in TEM6. The revised TEM estimates thawed SOC in different depths (SOC$_{PF1}$, SOC$_{PF2}$, …, SOC$_{PFn}$) and decomposition affected by environmental conditions in different layers (Env$_{lyr1}$, Env$_{lyr2}$, …, Env$_{lyrn}$).

simulates soil thermal dynamics for thawed and frozen soils and the effects of freeze-thaw dynamics on gross primary production (GPP) is given in Text S1 in Supporting Information S1.

With the degradation of permafrost, more frozen soil organic matter would be available for decomposition, which has been considered in TEM. The amount of SOC available for decomposition was calculated as a proportion of the entire rooting zone SOC, depending upon the ratio of active layer thickness (ALT) to rooting depth (Hayes et al., 2014; Kicklighter et al., 2019). As the rooting depth (z_r) in TEM is calculated by $z_r = z_a \cdot p_{si+cl}{}^2 + z_b * p_{si+cl} + z_c$ (where z_a, z_b, and z_c are vegetation type specified parameters, p_{si+cl} is the proportion of silt and clay), it does not change with time, nor increases as ALT increases. Previous versions of TEM did not consider SOC below the rooting zone and assumed that they do not contribute to C fluxes. When warming continues in the future and the active layer deepens below the rooting depth, this approach may underestimate the influence of permafrost degradation on the availability of carbon for decomposition (Hayes et al., 2011). Moreover, TEM calculated the SOC decomposition rate for the whole active layer affected by temperature and moisture of topsoil (about 20 cm) and did not consider the vertical variations in SOC turnover time, which may overestimate the SOC decomposition rate at depth to some extent (Shu et al., 2020).

In this study, we modified TEM (Figure 1) to represent C exposure and decomposition with permafrost thaw. Unlike previous versions of TEM, in which SOC from thawed permafrost layers was calculated as a proportion of SOC in the rooting zone, the modified model in this study calculated thawed SOC only according to active layer depth and thus were not constrained by rooting depth. The decomposition regime of thawed SOC was also modified to account for soil conditions in different depths:

$$RH_k = K_d C_{Sk} f(M_{Vk}) \exp(0.069 H_{Tk}) f(z_k) \tag{1}$$

where k is the index for thawed permafrost layer, K_d is a rate-limiting parameter that defines the rate of decomposition at 0°C, C_{Sk} is the amount of SOC in layer k, M_{Vk} is mean monthly volumetric soil moisture in layer k, and the function $f(M_{Vk})$ is a nonlinear relationship that models the effects of desiccation on microbial activity at low M_V and the influence of oxygen availability on microbial activity at high M_V, with an optimum at an intermediate level of M_V (Tian et al., 1999). H_{Tk} is the mean monthly temperature (can be less than 0°C) of the thawed permafrost layer k simulated by the soil thermal model. A possible explicit depth dependence, $f(z_k)$, was introduced to TEM in this study to account for processes other than temperature, moisture, and anoxia that can limit decomposition, such as priming effects, microscale anoxia, soil mineral surface, and aggregate stabilization. These unresolved depth controls were represented by an exponential decrease function of the soil turnover time with depth, $\exp(-z_k/z_\tau)$, where z_k is the depth of the thawed permafrost layer k, and z_τ is the e-folding depth of intrinsic turnover rates (Koven et al., 2013).

2.2. Observationally-Constrained Model Initialization for Permafrost Carbon Storage

Based on field observations, SOC profiles along soil depth have been mapped for the Arctic (Hugelius et al., 2014; Mishra et al., 2021) and the Qinghai-Tibetan Plateau (Ding et al., 2016; Wang et al., 2020). Integrating these observational-based SOC profiles into land surface models could reduce the uncertainties in model initial values for SOC content in different soil depths (Burke et al., 2017; Jafarov & Schaefer, 2016; Schneider von Deimling et al., 2015), which are normally determined during model spin-up and can differ from observations. Here, the observational-based SOC profiles from the Arctic and the Qinghai-Tibetan Plateau were used as the initial value for SOC content in frozen layers in 2015. Before 2015, we assume these SOC freezing in deep soils and keeping constant. When the active layer deepens after 2015, the amount of thawed SOC in the corresponding layers can be calculated according to the observational-based SOC profiles, which is noted as SOC_{PFn} in Figure 1. Note that observational-based SOC profiles only have four layers, 0−30 cm, 30−100 cm, 100−200 cm, and 200−300 cm. There are 25 permafrost layers for the modified TEM, with 10 cm intervals for 0−1 m, 20 cm intervals for 1−3 m, 50 cm intervals for 3−5 m, and one layer for 5−6 m. We assume an even SOC content distribution for each observational-based SOC layer. For model layers shallower than 3 m, SOC content is calculated as a fraction of the corresponding observational-based SOC layer, and for layers deeper than 3 m, SOC content is calculated from a hyperbolic function fitted by 0–3 m observational SOC data at the same location. For model grids without observations, the SOC content of model layers is calculated from a hyperbolic function fitted by observational SOC data of the same plant function type (Figure S1 in Supporting Information S1).

Permafrost degradation influences not only the amount of SOC but also soil organic N (SON) and available inorganic N. We assume the addition of N from thawing permafrost follows the same hyperbolic relationship with soil depth as SOC. However, although permafrost degradation can increase available N pools, we assume that the additional N cannot be accessed to vegetation if ALT deepens far below rooting depth. Therefore, only N in the rooting zone was available for vegetation N uptake when ALT is deeper than the rooting zone depth.

2.3. Regional Simulation

TEM simulations are conducted at a monthly time step and a 0.5-degree latitude by 0.5-degree longitude spatial resolution for the pan-Arctic permafrost regions and mountain regions such as the Tibet Plateau. Spatially referenced information on climate, soils, vegetation, and elevation drives TEM. Climate data, including air temperature (°C), precipitation (mm), and incident shortwave solar radiation (W m^{-2}) from 1850 to 2100, were derived from the GFDL-ESM4 global circulation model in the third simulation round of the Inter-Sectoral Impact Model Intercomparison Project (ISIMIP 3b). Based on the output of phase six of the Coupled Model Intercomparison Project (CMIP6; Eyring et al., 2016), climate data in the ISIMIP 3b have been bias-adjusted and statistically downscaled with the observational referenced data set W5E5 (Cucchi et al., 2020; Lange, 2019). Regional simulations of this century (2015–2100) were conducted under three climate scenarios SSP1-RCP2.6 (the Shared Socioeconomic Pathway 1 (SSP1; O'Neill et al., 2017) and Representative Concentration Pathway 2.6 (RCP2.6; Moss et al., 2010)) and SSP5-RCP8.5 (SSP5 and RCP8.5), hereinafter referring to as SSP126 and SSP585, respectively. Climate data of the historical scenario was used for model simulations from 1850 to 2015. Yearly global mean CO_2 concentrations for historical and 21st-century periods are derived from the Earth System Grid Federation servers (https://esgf-node.llnl.gov/projects/%20input4mips/). During the simulation, atmospheric CO_2 concentrations are the same for every month and every model grid in a specific year.

Soil texture and elevation data over the permafrost region were based on the Regirded Harmonized World Soil Database v 2.0 (https://gaez.fao.org/pages/hwsd) and the ALOS World 3D-30 m (AW3D30) digital surface model data set (Takaku et al., 2020), respectively. The vegetation data set were set the same as Zhuang et al. (2011), which divided global vegetation into 35 types, and the distribution of vegetation types in northern high latitudes is shown in Figure S2 in Supporting Information S1. The soil texture, elevation, and vegetation data were grided to a spatial resolution of 0.5° as the climate data. Daily climate data were averaged to a monthly scale before applying to model simulations.

For each grid cell, the model was first runup to 3,000 years to reach equilibria for water, C, and N fluxes and pools with climate data of 1850 repeatedly. C and N pools of the equilibrium state were then used as the initial value for

Table 1
Description of FLUXNET2015 Sites Used for Model Calibration (1–3) and Validation (4–9)

	Site ID	Site name	Latitude (°)	Longitude (°)	Elevation (m)	Vegetation type	Date range
1	US-Prr	Poker Flat Research Range	65.124	−147.488	210	Boreal forest	2011–2012
2	US-Atq	Atqasuk	70.470	−157.409	15	Wet tundra	2004–2006
3	GL-ZaH	Zackenberg Heath	74.473	−20.550	38	Polar desert	2006–2008
4	RU-SkP	Yakutsk Spasskaya Pad larch	62.255	129.168	246	Boreal forest	2014–2014
5	US-Prr	Poker Flat Research Range	65.124	−147.488	210	Boreal forest	2011–2012
6	US-Atq	Atqasuk	70.470	−157.409	15	Wet tundra	2007–2008
7	US-Ivo	Ivotuk	68.487	−155.750	568	Wet tundra	2004–2007
8	GL-ZaH	Zackenberg Heath	74.473	−20.550	38	Polar desert	2009–2011
9	CN-Dan	Dangxiong	91.066	30.498	4,295	Alpine tundra	2007–2010

model spin-up, using the forcing data from 1850 to 1860 repeatedly for 500 years. After this, a historical simulation from 1850 to 2014 was run before performing transient simulations from 2015 to 2100.

2.4. Model Parameterization

Most of the parameters in TEM are assigned values derived from the literature, but some parameters are calibrated to the C and N pools and fluxes of intensively studied sites (McGuire et al., 1992; Raich et al., 1991; Zhuang et al., 2011). Due to the modification of the model structure in this study, key parameters related to ecosystem C and N cyclings, such as the maximum rate of photosynthesis, heterotrophic respiration, plant N uptake, autotrophic respiration rate, and soil N immobilization (Zhu & Zhuang, 2014), were recalibrated. Following Zhuang et al. (2011), three ecosystem communities were considered, including boreal forest, wet tundra and polar desert and alpine tundra. Boreal forests include both deciduous and coniferous forests. The model was parameterized and then extrapolated based on regional distribution of these ecosystem types. These parameters were optimized using the PEST (Parameter ESTimation; Welter et al., 2015) software package. PEST optimizes model parameters by an iterative method based on the Gauss-Marquardt-Levenberg (GML) gradient search algorithm. This algorithm has both the global search capability of gradient descent and the fast convergence of the Gauss-Newton method, and can quickly achieve the solutions for the objective function with a few model runs. Other parameters, such as the ones regulating heat transfer in the soil profile and hydrological processes, and the ones configuring model running, were set as default values (Zhuang et al., 2011). Calibrated parameters and their optimal values are listed in Table S1 in Supporting Information S1. Observation sites (Table 1) used for model calibration and parameter verification were derived from the FLUXNET2015 data set (Pastorello et al., 2020).

2.5. Simulation Protocol

To investigate the effects of key factors including permafrost degradation, evaluating atmosphere CO_2 concentration, changing temperature and precipitation, as well as their interactions on carbon sequestration in the permafrost areas, factorial runs were conducted as shown in Table 2. For each factor (or each pair of factors), a referenced simulation was carried out, in which the factor of interest (or factor pair) was kept at the 2015 value for the entire 2015–2100 period, and the other factors remained unchanged as their original future scenario. Apart from the referenced simulations, a transient simulation was also conducted, in which all the factors were kept as their original future scenario data. The effects of an individual factor (or factor pair) on the simulation results can then be approximated by subtracting the results of the corresponding referenced simulation from the transient simulation. All the transient and referenced simulations were conducted under SSP126 and SSP585 for the 21st century. Therefore, there were 20 simulations in total.

3. Results

3.1. Model Validation

TEM was calibrated with monthly observations of soil temperature, GPP, ecosystem respiration, and net ecosystem production (NEP) for boreal forest, wet tundra, and polar desert in the Northern Hemisphere

Table 2
Simulation Design to Investigate the Effects of Active Layer Deepening, Climate Change, Increasing Atmospheric CO_2, and Nitrogen Deposition on Carbon Cycling in the Northern High Latitude Permafrost Regions

Simulations	Permafrost	CO_2	Temperature	Precipitation
S_{Trans}	1850–2100	1850–2100	1850–2100	1850–2100
S_{PF}	**1850–2015**	1850–2100	1850–2100	1850–2100
S_{CO2}	1850–2100	**1850–2015**	1850–2100	1850–2100
S_{Temp}	1850–2100	1850–2100	**1850–2015**	1850–2100
S_{Prec}	1850–2100	1850–2100	1850–2100	**1850–2015**
$S_{PF\&CO2}$	**1850–2015**	**1850–2015**	1850–2100	1850–2100
$S_{PF\&Prec}$	**1850–2015**	1850–2100	1850–2100	**1850–2015**
$S_{CO2\&Temp}$	1850–2100	**1850–2015**	**1850–2015**	1850–2100
$S_{CO2\&Prec}$	1850–2100	**1850–2015**	1850–2100	**1850–2015**
$S_{Temp\&Prec}$	1850–2100	1850–2100	**1850–2015**	**1850–2015**

Note. S_{Trans} denotes the transient simulation, and S_{PF}, S_{CO2}, S_{Temp}, and S_{Prec} denote the referenced simulation with constant active layer thickness, atmospheric CO_2 concentration, air temperature, and precipitation at the 2015 level for the entire 2015–2100 period, respectively. Simulations with two factors aim to investigate the effects of the interactions of these two factors on permafrost carbon sequestration. The bold values mean that the corresponding factor (of factor pair) changed with time during 1850–2015 but was kept at the 2015 value for the entire 2015–2100 period.

permafrost region (Figure 2 and Figure S3 in Supporting Information S1). Then the model was validated for the three dominant ecosystems at different sites or the same site in different years (Figure 3 and Figure S4 in Supporting Information S1). TEM well reproduced the seasonal variation of soil temperature and C fluxes at all sites, with R^2 for soil temperature close to 0.9 in model calibration and greater than 0.7 in model validation, and R^2 for NEP greater than 0.7 in model calibration and ranging from 0.69 to 0.93 in model validation. R^2 for NEP is normally smaller than that for GPP and ecosystem respiration because the change in NEP is the result of the variation of GPP and ecosystem respiration and is affected by more complex processes (Junttila et al., 2021; Niu et al., 2021).

Permafrost area for the Northern Hemisphere permafrost region during 2010–2015 is estimated at 14.4×10^6 km^2, which is located in the middle of the estimation of Liu et al. (2021; $14.9 \pm 0.2 \times 10^6$ km^2) and Obu et al. (2019; 13.9×10^6 km^2), but lower than the estimation of 16.2×10^6 km^2 given by Slater and Lawrence (2013). Total SOC stocks in the active layer of the Northern Hemisphere permafrost region were estimated as 563 Pg C in 2015, which is comparable to ~500 Pg estimated by Hugelius et al. (2014). Our estimation of vegetation C stocks in 2015 (98 Pg C) is lower than the mean value of 126 ± 64 (mean ± SD) Pg C estimated by McGuire et al. (2018) but close to an observational-based estimation of vegetation C in tundra and boreal biomes (55 Pg C; Neigh et al., 2013; Raynolds et al., 2012).

3.2. Changes in Permafrost and C Balance During the 21st Century

The Permafrost area (defined here as ALT less than 10 m) of the Northern Hemisphere is projected to shrink in the 21st century (Figure 4a). Under the SSP126, permafrost area would decrease gradually in the entire century, but it

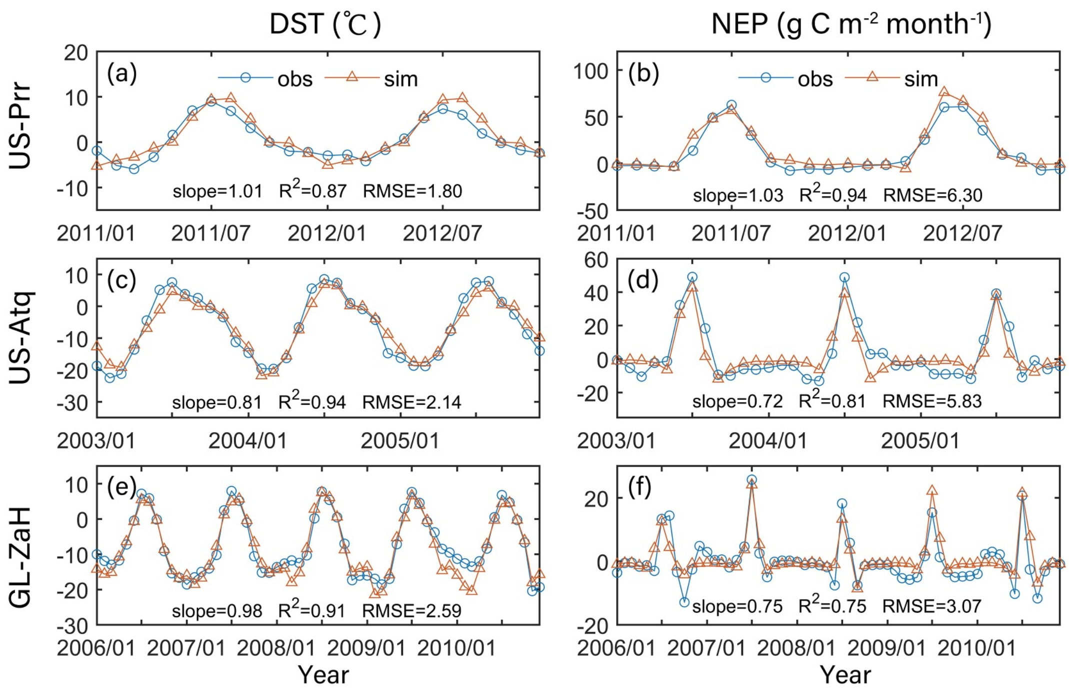

Figure 2. Calibration of Terrestrial Ecosystem Model at three dominant ecosystems of the Northern Hemisphere permafrost region for soil temperature at 10 cm (DST) and net ecosystem production. US-Prr, US-Atq, and GL-ZaH are observation sites for boreal forests, wet tundra, and polar desert, respectively. Refer to Table 1 for site information.

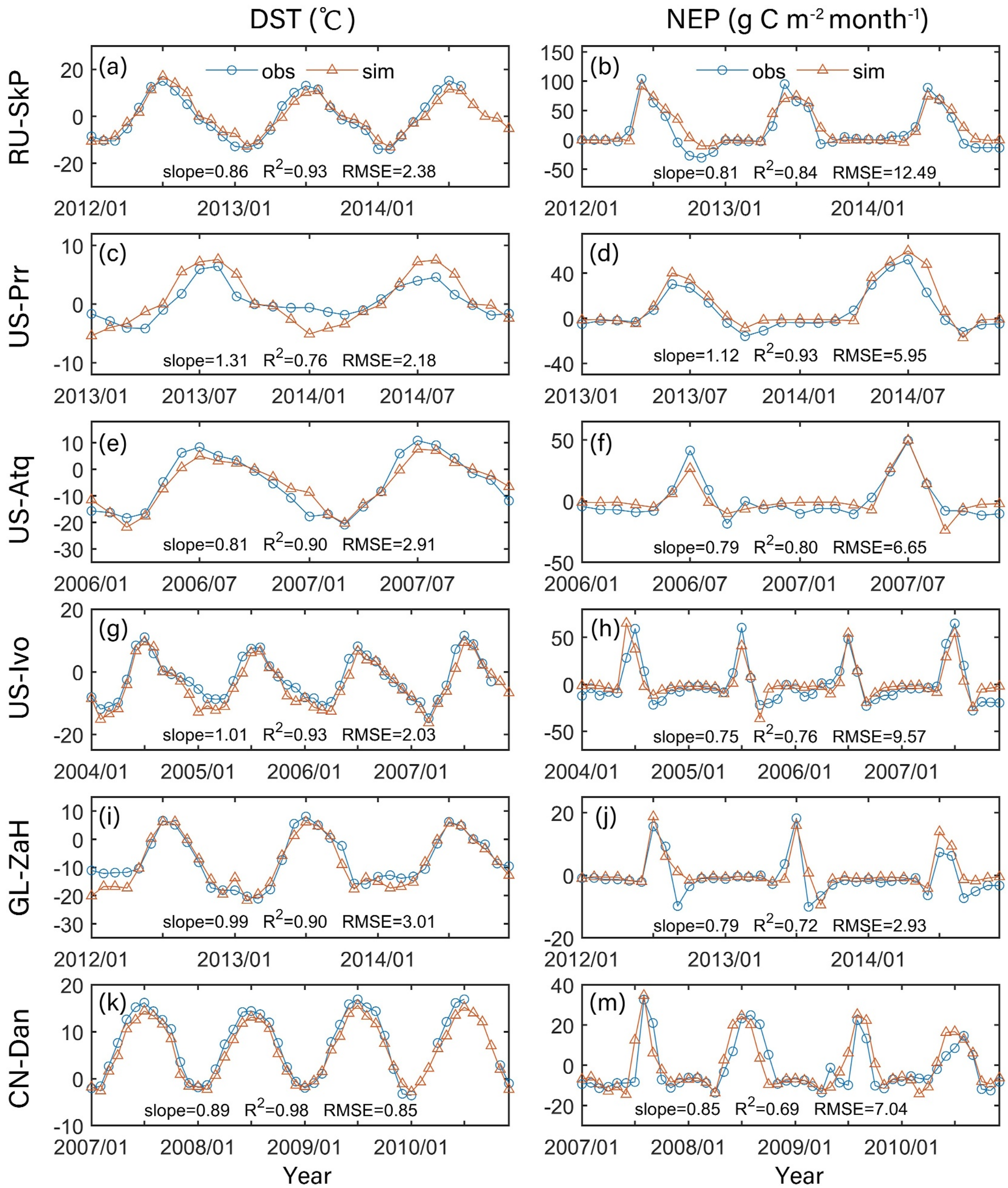

Figure 3. Model validation for Terrestrial Ecosystem Model at three dominant ecosystems of the permafrost region of the Northern Hemisphere for soil temperature at 10 cm (DST) and net ecosystem production. RU-SkP and US-Prr are boreal forest observation sites; US-Atq and US-Ivo are wet tundra observation sites; and GL-ZaH and CN-Dan are polar deserts or alpine tundra sites. Refer to Table 1 for site information.

would drop exponentially after 2060 under the SSP 585. By 2100, permafrost area would decrease by 1.45×10^6 and 2.57×10^6 km^2 under the SSP126 and SSP585, respectively. Similarly, the active layer deepens gradually under the SSP126 but more rapidly under the SSP585 (Figure 4b). By 2100, ALT would increase by 1.02 and 3.80 m under the SSP126 and SSP585, respectively.

Both NPP and RH would increase in the future under the SSP126 and SSP585 scenarios, with a steeper rise under the SSP585 (Figure 4c). Most of the time, NPP under both SSP scenarios is greater than RH, resulting in a net C sink (a positive NEP in Figure 4c), except for a weak C source at the end of the 21st century under the SSP126. Moreover, the rates of C loss from thawed permafrost increase steadily with warming, which diminishes the carbon sink ability of the permafrost areas (Figure S5 in Supporting Information S1). Under the SSP585, C

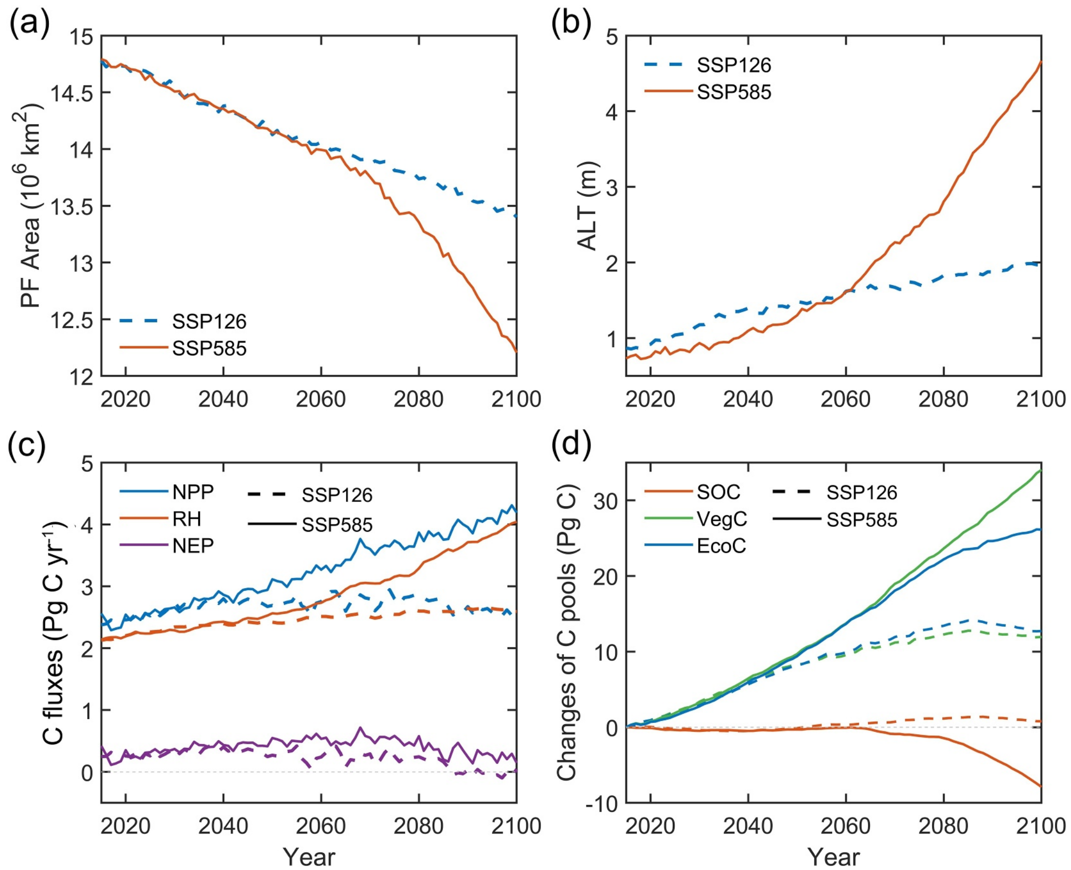

Figure 4. Projections of permafrost area (a), active layer thickness (ALT; b), C fluxes (c), and the changes of C pools relative to 2015 (d) in the Northern Hemisphere permafrost area during 2015–2100 under the SSP126 and SSP585 scenarios. SOC, VegC, and EcoC in panel (d) are soil organic C, vegetation C, and ecosystem C stocks, respectively.

released from the decomposition of newly thawed permafrost in the 2090s accounts for 18% of total ecosystem RH. If these C emissions are not considered, NEP as a carbon sink during this period could triple (increase from 0.26 to 0.91 Pg C yr^{-1}). Vegetation would gain more C due to increasing NPP (Figure 4d). SOC sizes would change slightly under the SSP126 but would reduce steadily after 2060 under the SSP585. However, soil C losses under the SSP585 are smaller than vegetation C gains, increasing ecosystem C stocks by 26.13 Pg by 2100. Under the SSP126, increasing vegetation and soil C stocks results in ecosystem C stocks accruing by 12.72 Pg by 2100.

3.3. Effects of Permafrost Degradation on the Ecosystem C Balance

The only difference between the transient (S_{Trans}) and the referenced (S_{PF}) simulations is that ALT was kept constant after 2015 in S_{PF} but varied with climate change in S_{Trans}. Therefore, the effects of ALT deepening on ecosystem C balance of the Northern Hemisphere permafrost regions can be approximated by subtracting the results of S_{PF} from S_{Trans}. Permafrost degradation has pronounced influences on C fluxes and pools during 2015–2100 (Figure 5). By the end of this century, permafrost degradation would expose 119.3 Pg and 251.57 Pg frozen C under the SSP126 and SSP585, respectively. RH in 2100 would increase by 0.10 Pg C yr^{-1} (SSP126) and 0.77 Pg C yr^{-1} (SSP585) compared to that in 2015 (Figure 5a). Cumulatively, permafrost degradation in this century would increase RH by 5.55 Pg C and 20.68 Pg C under the SSP126 and SSP585, respectively. Permafrost degradation has limited effects on RH in the active layer but stimulates RH from thawed permafrost significantly (Figure 5). Cumulatively, RH from thawed permafrost in this century accounts for 18% and 31% of total increased RH under the SSP126 and SSP585, respectively.

Although permafrost degradation increases SOC in the active layer (Figure 5b), the increases are much smaller than the decrease of SOC in the previously frozen layers due to C decomposition. SOC in the entire soil profile,

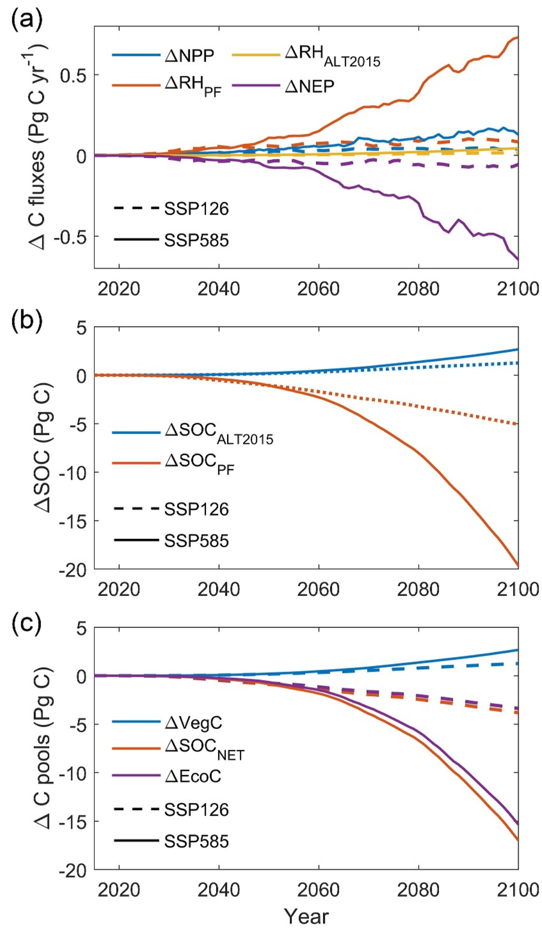

Figure 5. The single effects of permafrost degradation on ecosystem C fluxes and pool sizes of the Northern Hemisphere permafrost areas during 2015–2100 under the SSP126 and SSP585. Δ denotes the differences between the transient (S_{Trans}) simulation and the referenced one (S_{PF}) in which active layer thickness is kept constant (S_{Trans}-S_{PF}). $RH_{ALT2015}$ in panel (a) is RH from the chunk of soils with fixed depth which are active layer depths in 2015. RH_{PF} is RH from thawed permafrost that was frozen in 2015. $\Delta SOC_{ALT2015}$ in panel (b) is the increase of SOC in the chunk of soils that are active layers in 2015 and ΔSOC_{PF} represents the change of SOC in thawed permafrost that is frozen in 2015. ΔSOC_{NET} in panel (c) is the change of total SOC in the active and frozen layers. ΔEcoC is the change of total ecosystem C (vegetation C and SOC) in the permafrost areas.

therefore, would decrease under all the SSPs (Figure 5c). By 2100, SOC in the previously frozen layers (SOC_{PF}) would decrease by 5.06 Pg and 19.66 Pg, which accounts for 4% and 8% of newly thawed permafrost C under the SSP126 and SSP585, respectively, indicating that most of the thawed SOC would remain in previously frozen layers in this century due probably to undesirable decomposition conditions in deep soils.

The stimulation effects of permafrost degradation on NPP are relatively small (Figure 5a). Compared to that in 2015, NPP by the 2090s would only increase by 0.04 Pg C yr^{-1} and 0.15 Pg C yr^{-1} under the SSP126 and SSP585, respectively. Cumulatively, NPP would increase by 2.18 Pg C (SSP126) and 5.34 Pg C (SSP585). As the result of the smaller increases in NPP than RH, NEP would decrease by 0.07 Pg C yr^{-1} (SSP126) and 0.53 Pg C yr^{-1} (SSP585) by the 2090s, and ecosystem C stock would reduce by 3.37 Pg (SSP126) and 15.37 Pg (SSP585) during 2015–2100 (Figure 5c).

The amount of SOC exposed from thawed permafrost decreases along soil depth except for 0−1 m. The amount of thawed SOC in 0–1 m is relatively small, because many permafrost areas currently have ALT greater than 1 m, and when permafrost thaws in these areas, SOC below 1 m would be exposed. Thawed SOC is mainly located 1−3 m, accounting for nearly half (47% and 49% under the SSP126 and SSP585, respectively) of the total thawed SOC in 0–6 m. Only a small fraction of thawed SOC would be decomposed through RH during 2015–2100 (Figure 6). The proportion of decomposed SOC tends to decrease along soil depth. In deep soils, the decomposition of SOC may be suppressed due to low oxygen, small microbial biomass, and low microbial activities with cold temperatures (Dash et al., 2019; Gross & Harrison, 2019; Kirschbaum et al., 2021). Thawed SOC in 1–2 m would decompose fast under both SSP scenarios, contributing to 35% and 43% of all the C emissions from 0 to 6 m. Soil conditions in 0–1 m should be the most favorable for SOC decomposition, but the decomposition is relatively small (Figure 6). This is because SOC exposed from 0 to 1 m is located in areas where ALT is smaller than 1 m currently. These areas are mainly cold permafrost regions, and their low soil temperature suppresses the decomposition of newly thawed SOC, resulting in a small fraction of C emission through RH. However, it should be noted that compared to SSP126, higher warming in SSP585 would cause greater decomposition of thawed SOC in the entire soil profile.

3.4. Analysis of Major Controls on Carbon Balance

The single effects of permafrost degradation, elevating atmospheric CO_2 concentration, changing precipitation and air temperature, as well as the combined effects of their interactions on ecosystem C balance are approximated by subtracting the results of the corresponding referenced simulation from the transient one (Table 1, Figure 7). Permafrost degradation, warming, and increasing precipitation (Figure S6 in Supporting Information S1) under the SSP126 and SSP585 promote NPP but have more pronounced effects on RH. As a result, they have limited benefits to vegetation C stocks but decrease SOC remarkably. Elevating atmospheric CO_2 concentration, however, stimulates NPP significantly and increases vegetation C stocks noticeably under both scenarios. Even with enhanced RH, SOC stocks still increase markedly owing to intensified litterfall under increasing vegetation C stocks. By 2100, CO_2 fertilization would boost ecosystem C stocks by 12.13 Pg C and 56.50 Pg C under the SSP126 and SSP585 scenarios, respectively, outweighing the negative effects caused by the change of precipitation and air temperature under both scenarios.

The combined effects of the factors on NPP are normally greater than a single factor (Figure 7a), indicating that permafrost degradation, eCO_2, warming, and increasing precipitation would promote NPP collectively in the future. However, there is one exception, the combination of warming and eCO_2 under the SSP585 has slightly

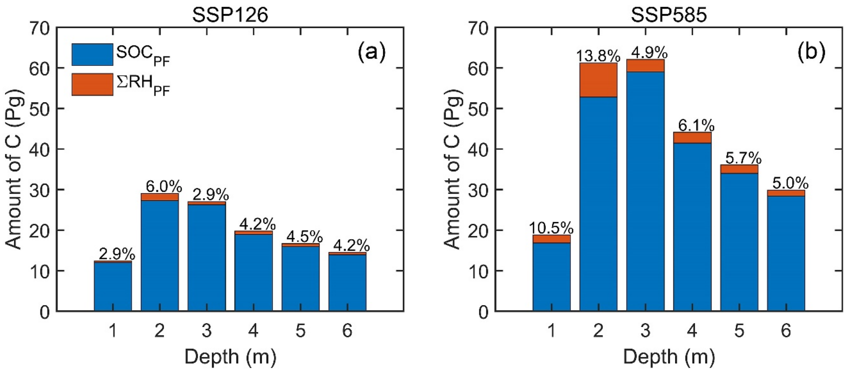

Figure 6. SOC released from thawed permafrost and their decomposition along soil depth. SOC_{PF} is the amount of SOC released from thawed permafrost by 2100, and $\sum RH_{PF}$ is cumulative RH from thawed permafrost during 2015–2100. The numbers above each bar are the fraction of thawed SOC that is decomposed through RH during 2015–2100.

smaller effects on NPP than the single eCO_2. High warming under the SSP585 may result in water stress and hinder the increase in NPP, which can be supported by the greater combined effects of eCO_2 and increasing precipitation than the single effects of eCO_2, and by the biggest combined effects of warming and eCO_2 under low

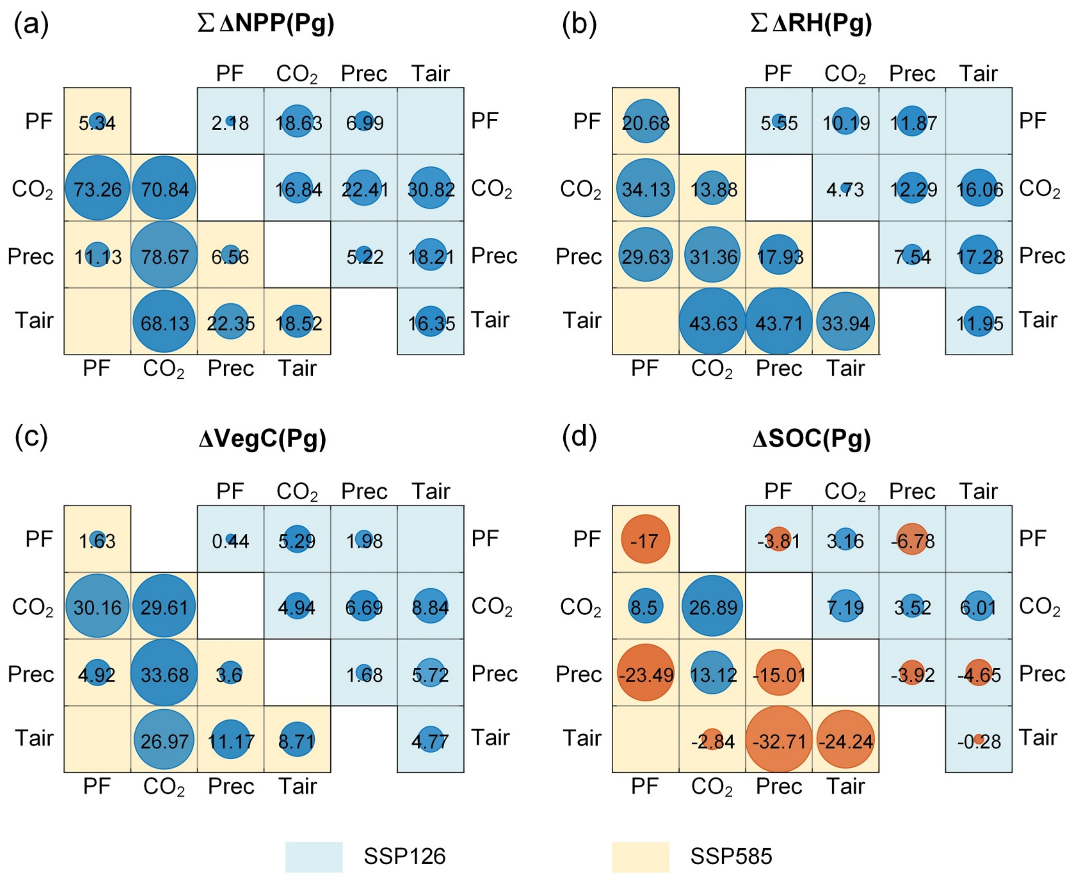

Figure 7. Effects of permafrost degradation (PF), elevating atmospheric CO_2 concentration (CO_2), changing precipitation (Prec) and air temperature (Tair) on ecosystem C fluxes (NPP and RH, (a) and (b) respectively) and pool sizes (SOC and vegetation C (VegC) stocks, (c) and (d) respectively) of the Northern Hemisphere permafrost regions during 2015–2100 under the SSP126 and SSP585 scenarios. Grids with rows and columns sharing the same variable represent the single effect of that specific variable, otherwise denote the combined effects of the rows and columns. Δ before the variables denote the differences between the transient simulation and the referenced one (see Table 2). ∑ in (a) and (b) are the cumulative differences from 2015 to 2100.

warming in SSP126. Enhanced NPP promotes vegetation C stock. As a result, the combined effects of the factors on vegetation C stock show the same pattern as those on NPP (Figure 7c), with the combination of warming and eCO_2, and the combination of increasing precipitation and eCO_2 increasing vegetation C stock the most under the SSP126 and SSP585, respectively.

All the combined effects of the factors on RH are greater than a single factor (Figure 7b). The combination of warming and increasing precipitation has the biggest effects on RH under both SSP126 and SSP585. The intensified RH under warming and increasing precipitation finally caused a remarkable reduction in SOC stocks (Figure 7d). The combination of warming and eCO_2 has the second largest effect on RH (Figure 7b) under both SSPs. eCO_2 stimulates plant growth, producing more litterfall and root exudates, and supplying RH with more substrates. Therefore, the combination of warming and eCO_2 enhances RH more greatly than warming. The combination of eCO_2 with warming and increasing precipitation both diminish the positive effects of eCO_2 on SOC stocks due to enhanced RH (Figure 7d).

4. Discussion

4.1. Permafrost Carbon Decomposition in Deep Soils

Permafrost degradation in the Northern Hemisphere would expose a large amount of previously frozen SOC, but most of them would be retained in soils during this century, especially in deep soil layers (Figure 6). The decomposition of thawed SOC is determined by the interactions of SOC compounds (particulate or mineral-associated organic carbon), the biotic factors of microbial communities and plant-microbe interactions, the abiotic environment of soil temperature, moisture, texture, pH, nutrient availability, and the physical and chemical protection of organic matter (Conant et al., 2011; Haddix et al., 2020; Lehmann et al., 2020; Witzgall et al., 2021). A synthesis of long-term (>1 year) aerobic soil incubations from the circumpolar permafrost area (Schädel et al., 2014) found that slow C pool decreased significantly toward deep mineral soils, and up to 90% of the total C pool was passive C in deep soils. As a result, SOC decomposability was higher in shallow than in deeper mineral soils. In addition, lower below-ground biomass and therefore smaller rhizosphere priming effects, decreased carbon-to-nitrogen (C:N) ratio, occlusion within soil aggregates, and physical protection by soil minerals all contribute to the lower SOC decomposability in deep soils (Hicks Pries et al., 2018; J. Li et al., 2018; Rumpel & Kögel-Knabner, 2011).

4.2. Effects of Permafrost Degradation on Ecosystem C Cycling

119.30 Pg and 251.57 Pg permafrost C would be exposed from previously frozen soils under the SSP126 and SSP585, respectively. These projections of exposed C are greater than the estimation of a perturbed physics ensemble (MacDougall & Knutti, 2016), which estimated that the permafrost areas might release 56 (13–118) Pg C under the RCP 2.6, and 102 (27–199) Pg C under the RCP 8.5 by 2100. The greater estimation in our study mainly results from deeper soil layers. The study of MacDougall and Knutti (2016) calculated thawed C dynamics in 0–3 m, while permafrost C in 0–6 m is considered in our study. When only 0–3 m is considered, exposed C would be 56.05 Pg (SSP126) and 123.25 Pg (SSP585), very close to the estimation of MacDougall and Knutti (2016). The decomposition of these newly-thawed SOC would stimulate RH significantly (Figure 5a) and cumulatively release 5.06 Pg (SSP126) and 19.66 Pg (SSP585) permafrost C into the atmosphere by 2100, accounting for 5% (SSP126) to 8% (SSP585) of the total thawed C. An expert judgment is that 5%–15% of the terrestrial permafrost C pool will be released into the atmosphere during this century (Schuur et al., 2015). Our projection is relatively low but still comparable to this expert judgment. Some processes like thaw slumps, cryoturbation, thermokarst development, and abrupt thaw may accelerate permafrost degradation in deep soils (Miner et al., 2022; Turetsky et al., 2020), and some other processes like root deepening and microbial colonization may promote the decomposition of deep SOC (Blume-Werry et al., 2019; Monteux et al., 2020). The missing of these processes in this study may result in a lower estimation of SOC decomposition in deep soils.

Permafrost degradation, on the other hand, would increase N availability. Under the SSP126 and SSP585 scenarios, permafrost degradation would expose 10.73 Pg and 27.20 Pg soil organic N, respectively. These additional N would promote net N mineralization, increase N availability, strengthen NPP (Figure 5a), and finally increase vegetation N stocks by 9.97 Tg and 26.17 Tg, and vegetation C stocks by 0.44 Pg and 1.63 Pg under the SSP126 and SSP585, respectively. The positive effects of permafrost degradation on vegetation growth through the increasing N availability have been observed previously, by Finger et al. (2016) and Blume-Werry et al. (2019).

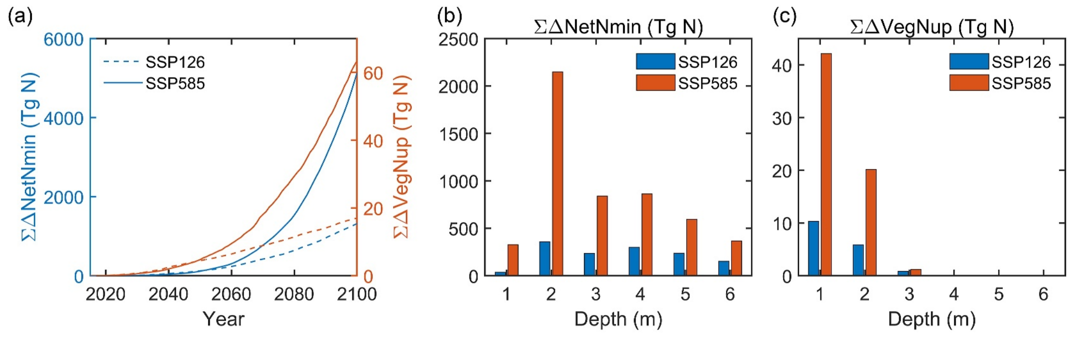

Figure 8. The single effects of permafrost degradation on net N mineralization (NetNmin) and vegetation N uptake (VegNup) with time (a) and along soil depth (b and c). Δ before the variables denote the differences between the transient simulation and the referenced one with constant active layer thickness (see Table 2). ∑ is the cumulative difference from 2015 to 2100.

Recently, a 20-year survey across 14 sites on the Tibetan Plateau (Yun et al., 2023) demonstrated again that permafrost thaw with corresponding released ammonium can be an important source of inorganic N for plants, and combined with active layer warming, permafrost thaw has led to significant changes in plant species composition and growth.

However, the increases in vegetation C stocks stimulated by additional N cannot fully compensate for the loss in SOC stocks due to enhanced RH after permafrost thaw, resulting in a net reduction of ecosystem C stock (Figure 5c). Similar results have also been found in high-latitude regions. In the boreal forest of Northern Eurasia, Kicklighter et al. (2019) found that the gain of vegetation C due to permafrost degradation only accounts for 29.8% and 49.2% of the loss of SOC under the RCP 4.5 and RCP 8.5, respectively. They claimed that although permafrost degradation provides increased N availability to enhance vegetation C uptake, this additional N comes at the cost of more synchronous losses of SOC. In the Pan-Arctic region, permafrost degradation exposed 11.6 Pg C of SOC and heightened CO_2 emission by 4.0 Pg during 1970–2006, but only 0.3 Pg C is compensated by enhanced vegetation CO_2 uptake (Hayes et al., 2014).

The limited benefits of N addition from thawed permafrost can be attributed to several reasons. First, N would not be abundant for vegetation in the permafrost areas. One of the TEM outputs is the NPP without N limitation. Figure S7 in Supporting Information S1 shows the benefit from N addition from thawed permafrost. NPP in transient simulations under both SSPs are higher than those in the simulations with constant ALT, but far below the NPP without N limitation, indicating that vegetation growth in the permafrost areas would still be constrained by N availability. Under the SSP126 and SSP585, the cumulative vegetation N uptake from thawed permafrost only takes up 1.3% and 1.2% of the cumulative net N mineralization, respectively (Figure 8a). Therefore, vegetation growth in permafrost areas is constrained by N, but N released from thawed permafrost cannot be utilized efficiently. Second, permafrost degradation can be deep in soils of mountain areas such as the Qinghai Tibetan Plateau, where ALT is averaged to be more than two m (Ni et al., 2021; Wang et al., 2020; X. Wu et al., 2018). However, the rooting depth of grasslands on the Qinghai Tibetan Plateau is generally shallower than 30 cm (Yang et al., 2009). N released from deep permafrost in the future could be far beyond plant accessibility. Figures 8b and 8c also shows that vegetation N uptake concentrates in the top 2 m, whereas a large fraction of net N mineralization takes place in soils deeper than 2 m. Third, it has been found that the benefits of enhanced net N mineralization on vegetation C uptake do not occur until the late 21st century (Kicklighter et al., 2019). Figure 8a shows that the build-up of net N mineralization in this study would only become evident after 2050 under the SSP126 and SSP585. Therefore, enhanced net N mineralization can only mitigate plant N limitation for a limited period. Furthermore, the phase lag of heat transfer into deep soils may shift the deep soil organic matter mineralization later into fall and winter, resulting in a seasonal offset from the peak period of N demand during spring and summer (Koven et al., 2015), and reducing the access of plant to the additional N released from deep permafrost thaw.

4.3. Effects of eCO_2 and Changing Climate

Elevated CO_2 (eCO_2) enhances photosynthesis by increasing the carboxylation rate of Rubisco and competitively inhibiting the oxygenation of Ribulose-1,5-bisphosphate (Drake et al., 1997). The single effects of eCO_2 boost

NPP substantially under the SSP126 and SSP585, leading to an increase in vegetation carbon stocks (Figure 7). A recent analysis (Keenan et al., 2023) that combined terrestrial biosphere models, ecological optimality theory, and remote sensing approaches found that CO_2 fertilization increased global annual terrestrial photosynthesis by 13.5 ± 3.5% or 15.9 ± 2.9 Pg C (mean ± s.d.) between 1981 and 2020. Evidence from four longest-running free-air CO_2 enrichment (FACE) experiments also show that eCO_2 increases biomass production and vegetation carbon stocks over a full decade in these early-succession temperate forests (Walker et al., 2019). However, in the later-succession forest at EucFACE, although 4 years of eCO_2 increased GPP by 12%, this additional carbon uptake did not lead to increased carbon sequestration at the ecosystem level (Jiang et al., 2020). Nutrient limitations have been considered to modulate the local magnitude of the eCO_2 effect on plant biomass (Ellsworth et al., 2017; Terrer et al., 2019; Walker et al., 2021). In earlier-succession ecosystems which tend to have higher nutrient availability, biomass production gains under eCO_2 are supported by increased N acquisition (Zaehle et al., 2014). However, in later-succession forests, some of which were severely limited by nutrients, biomass production shows no response to eCO_2 due to N (Sigurdsson et al., 2013) and phosphorus (Ellsworth et al., 2017) limitation. In this study, although N limitation on GPP is considered in TEM, phosphorus limitation and vegetation succession need to be developed and applied in the future to improve the estimation of CO_2 fertilization effects.

Figure 7 shows that eCO_2 would increase SOC stocks, owing to intensified litterfall under increasing vegetation C stocks. Meta-analysis of 53 experiments has demonstrated that eCO_2 increased litter production, carbon allocation below ground, and SOM decomposition rates (van Groenigen et al., 2014). The meta-analysis found that eCO_2 increased soil carbon stocks across more than 200 experiments (Hungate et al., 2009). However, 19 years of treatment application at BioCON (Pastore et al., 2021) found that there was no main effect of eCO_2 on total ecosystem C stocks and soil C pools, and increased soil C inputs were largely offset by enhanced soil CO_2 efflux. Data synthesized from 108 eCO_2 experiments (Terrer et al., 2021) suggest a negative relationship between SOC stocks and plant biomass under eCO_2. When plant biomass is strongly stimulated by eCO_2, SOC storage declines; conversely, when biomass is weakly stimulated, SOC storage increases. Nutrient constraints have been attributed to this trend. Under eCO_2, substantial acquisition of soil N is possible via priming effects in ectomycorrhizal fungi-associated plants, boosting vegetation growth at the expense of SOC stocks decrease. Low nutrient availability, on the contrary, strongly constrains the plant biomass sink in arbuscular mycorrhizal fungi-associated plants, but eCO_2 can trigger SOC accrual through plant carbon allocation belowground. Most models, including TEM in this study, focus on carbon inputs and decomposition processes but underestimate priming and rhizosphere effects, which may result in discrepancies between observations and models.

Warming and increasing precipitation would intensify RH and cause remarkable reductions in SOC stocks (Figure 7d). Although annual precipitation would increase under both SSPs (Figure S6 in Supporting Information S1), the volumetric soil moisture (of the top 20 cm of soil profile) is modeled to fluctuate slightly under the SSP126 but decrease gradually under the SSP585 (Figure S7 in Supporting Information S1), indicating a warmer and drier environment in the 21st century. As an important factor of soil environmental drivers associated with oxygen availability, soil moisture is tightly coupled to biogeochemical cycles (Cook & Orchard, 2008; Moyano et al., 2013). Many studies have demonstrated that the fate of thawed SOC highly depends on soil hydrology conditions (Göckede et al., 2019; F. Li et al., 2020; Pegoraro et al., 2021; Song et al., 2020; Yao et al., 2021). Wetting and the shortage of oxygen suppress microbial activities and dampen the loss of old permafrost C pools (Lupascu et al., 2014). By contrast, aerobic habitats with a high abundance of microorganisms could boost heterotrophic respiration and consume old permafrost C rapidly. The warmer and dryer environment projected in this study may stimulate decomposition and reduce SOC stocks. However, studies (Bond-Lamberty et al., 2016; Song et al., 2020) also found that permafrost C decomposition could be constrained by water stress, and low soil moisture conditions can reduce total soil C release by more than 30%. Although projected regional average soil moisture does not decrease much under the SSPs, drought on a local scale or continuous drying beyond 2100 may inhibit permafrost C emission.

4.4. Study Limitations

By integrating observation-based SOC profiles, permafrost degradation along soil depth, and associated C and N release, this study enhanced the credibility of permafrost C emission projections. Some processes like abrupt thaw, root deepening, and microbial colonization, however, may accelerate permafrost C emissions at depth. Abrupt thaw often causes much deeper permafrost to thaw more rapidly (Schuur et al., 2015) and could increase carbon emissions from permafrost by up to 40% (Turetsky et al., 2020). Apart from the abrupt thaw, it has been found that ground subsidence could increase the amount of newly thawed C by 37% under controlled experiments and by 113% under warming conditions (Rodenhizer et al., 2020). Strongly increased root growth and rooting depth could enhance plant interactions with thawing permafrost soil, and deep SOC that has long been locked up in permafrost is thus no longer detached from plant processes upon thaw (Blume-Werry et al., 2019). Microbial colonization can occur upon permafrost thaw. The change in microbial community composition can alleviate the functional limitations on C and N biogeochemical processes, initiating nitrification activities and increasing CO_2 production by 38% over 161 days (Monteux et al., 2020). All these processes should be coupled into land surface models to constrain our estimate uncertainties of the permafrost C feedback (Schädel et al., 2024).

The single effects of eCO_2 in this study are projected to increase both plant biomass and SOC stocks, and the accrual of SOC can be attributed to increased litter inputs due to enhanced plant production under eCO_2. However, Terrer et al. (2021) argued that a trade-off exists between the accumulation of plant biomass and SOC stocks under eCO_2 because of mycorrhizal fungi associated nutrient acquisition. They also examined the performances of 12 ecosystem models and found that none of the individual models was able to reproduce the observational trade-off between plant biomass and SOC storage. For more realistic modeling of the permafrost carbon cycle and more robust projecting of permafrost C feedback in the future, it is necessary to couple carbon-nutrient cycling mediated by plant-soil interactions into ecosystem models.

Projected future climate is also subject to high uncertainty (Tebaldi et al., 2021; C. Wu et al., 2021). Y. Wu et al. (2022) found that under the SSP585, the uncertainties (±1 standard deviation) of global annual mean temperature and precipitation by 2100 are projected to be 3.8°C and 243.8 mm, respectively, with the largest uncertainties for air temperature in regions of high latitudes and high altitudes. As a consequence, it can be relatively difficult to make reliable projections of future permafrost degradation and their impacts on ecosystem C cycling. Model parameters, which under most circumstances, are difficult to measure and estimate based on prior knowledge and available data (e.g., Jin et al., 2015; Zhuang et al., 2010); and equifinality that many different model structures and parameter sets may be acceptable in reproducing the observed behavior of the complex environmental system (Beven & Freer, 2001), are other major sources of simulation biases that need to be constrained in future studies.

5. Conclusions

A process-based biogeochemical model was refined by incorporating C exposure with permafrost thaw across soil profiles to quantify the impacts of permafrost degradation on ecosystem C balance in the Northern Hemisphere permafrost areas. We found that climate change would strengthen both NPP and RH and intensify C sequestration (NEP) in the permafrost region. Specifically, C exposed from thawed permafrost would stimulate decomposition, thereby increasing RH significantly. However, based on current simulation capabilities of the modified model, the N liberated from thawed permafrost may offer limited benefits to vegetation, resulting in a net C loss in this century due to permafrost degradation. Furthermore, the CO_2 fertilization effects are projected to boost NPP substantially, contributing to the accumulation of both vegetation C and SOC stocks. This study highlights the importance of the interactions between climate change, CO_2 fertilization, permafrost degradation, and associated C and N release on carbon-climate feedback assessments. Our projections indicate that most of the thawed SOC would remain in deep soil layers throughout this century. However, processes like abrupt thaw, root deepening, and microbial colonization may accelerate the decomposition of this vast amount of thawed SOC in deep soils. This study emphasizes the need for modeling communities to incorporate these processes into land surface models to better quantify permafrost C loss in deep soils.

Conflict of Interest

The authors declare no conflicts of interest relevant to this study.

Data Availability Statement

All model results in this study are available at Figshare https://doi.org/10.6084/m9.figshare.25705806 (Liu et al., 2024).

Acknowledgments

This study is funded by the National Natural Science Foundation of China (Grants 42301542 and 42271489) and the International Science and Technology Cooperation Project of Henan Province (Grant 242102520039). We thank the ISIMIP cross-sectoral science team for their roles in producing, coordinating, and making available the ISIMIP3b data (available at https://esg.pik-potsdam.de/search/isimip/).

References

Beven, K., & Freer, J. (2001). Equifinality, data assimilation, and uncertainty estimation in mechanistic modelling of complex environmental systems using the GLUE methodology. *Journal of Hydrology*, *249*(1), 11–29. https://doi.org/10.1016/S0022-1694(01)00421-8

Blume-Werry, G., Milbau, A., Teuber, L. M., Johansson, M., & Dorrepaal, E. (2019). Dwelling in the deep – Strongly increased root growth and rooting depth enhance plant interactions with thawing permafrost soil. *New Phytologist*, *223*(3), 1328–1339. https://doi.org/10.1111/nph.15903

Bond-Lamberty, B., Smith, A. P., & Bailey, V. (2016). Temperature and moisture effects on greenhouse gas emissions from deep active-layer boreal soils. *Biogeosciences*, *13*(24), 6669–6681. https://doi.org/10.5194/bg-13-6669-2016

Burke, E. J., Chadburn, S. E., & Ekici, A. (2017). A vertical representation of soil carbon in the JULES land surface scheme (vn4.3_permafrost) with a focus on permafrost regions. *Geoscientific Model Development*, *10*(2), 959–975. https://doi.org/10.5194/gmd-10-959-2017

Canadell, J. G., Monteiro, P. M. S., Costa, M. H., Cotrim da Cunha, L., Cox, P. M., Eliseev, A. V., et al. (2021). Global carbon and other biogeochemical cycles and feedbacks. In V. Masson-Delmotte, P. Zhai, A. Pirani, S. L. Connors, C. Péan, S. Berger, et al. (Eds.), *Climate Change 2021: The Physical Science Basis. Contribution of Working Group I to the Sixth Assessment Report of the Intergovernmental Panel on Climate Change* (pp. 673–816). Cambridge University Press.

Conant, R. T., Ryan, M. G., Ågren, G. I., Birge, H. E., Davidson, E. A., Eliasson, P. E., et al. (2011). Temperature and soil organic matter decomposition rates – Synthesis of current knowledge and a way forward. *Global Change Biology*, *17*(11), 3392–3404. https://doi.org/10.1111/j.1365-2486.2011.02496.x

Cook, F. J., & Orchard, V. A. (2008). Relationships between soil respiration and soil moisture. *Soil Biology and Biochemistry*, *40*(5), 1013–1018. https://doi.org/10.1016/j.soilbio.2007.12.012

Cucchi, M., Weedon, G. P., Amici, A., Bellouin, N., Lange, S., Müller Schmied, H., et al. (2020). WFDE5: Bias-adjusted ERA5 reanalysis data for impact studies. *Earth System Science Data*, *12*(3), 2097–2120. https://doi.org/10.5194/essd-12-2097-2020

Dash, P. K., Bhattacharyya, P., Roy, K. S., Neogi, S., & Nayak, A. K. (2019). Environmental constraints' sensitivity of soil organic carbon decomposition to temperature, management practices and climate change. *Ecological Indicators*, *107*, 105644. https://doi.org/10.1016/j.ecolind.2019.105644

Ding, J., Li, F., Yang, G., Chen, L., Zhang, B., Liu, L., et al. (2016). The permafrost carbon inventory on the Tibetan Plateau: A new evaluation using deep sediment cores. *Global Change Biology*, *22*(8), 2688–2701. https://doi.org/10.1111/gcb.13257

Drake, B. G., Gonzàlez-Meler, M. A., & Long, S. P. (1997). More efficient plants: A consequence of rising atmospheric CO_2? *Annual Review of Plant Physiology and Plant Molecular Biology*, *48*(1), 609–639. https://doi.org/10.1146/annurev.arplant.48.1.609

Ellsworth, D. S., Anderson, I. C., Crous, K. Y., Cooke, J., Drake, J. E., Gherlenda, A. N., et al. (2017). Elevated CO_2 does not increase eucalypt forest productivity on a low-phosphorus soil. *Nature Climate Change*, *7*(4), 279–282. https://doi.org/10.1038/nclimate3235

Eyring, V., Bony, S., Meehl, G. A., Senior, C. A., Stevens, B., Stouffer, R. J., & Taylor, K. E. (2016). Overview of the Coupled Model Intercomparison Project Phase 6 (CMIP6) experimental design and organization. *Geoscientific Model Development*, *9*(5), 1937–1958. https://doi.org/10.5194/gmd-9-1937-2016

Finger, R. A., Turetsky, M. R., Kielland, K., Ruess, R. W., Mack, M. C., & Euskirchen, E. S. (2016). Effects of permafrost thaw on nitrogen availability and plant-soil interactions in a boreal Alaskan lowland. *Journal of Ecology*, *104*(6), 1542–1554. https://doi.org/10.1111/1365-2745.12639?download=true

Foereid, B., Bellamy, P. H., Holden, A., & Kirk, G. J. D. (2012). On the initialization of soil carbon models and its effects on model predictions for England and Wales. *European Journal of Soil Science*, *63*(1), 32–41. https://doi.org/10.1111/j.1365-2389.2011.01407.x

Foster, A. C., Wang, J. A., Frost, G. V., Davidson, S. J., Hoy, E., Turner, K. W., et al. (2022). Disturbances in North American boreal forest and Arctic tundra: Impacts, interactions, and responses. *Environmental Research Letters*, *17*(11), 113001. https://doi.org/10.1088/1748-9326/ac98d7

Gay, B. A., Pastick, N. J., Züfle, A. E., Armstrong, A. H., Miner, K. R., & Qu, J. J. (2023). Investigating permafrost carbon dynamics in Alaska with artificial intelligence. *Environmental Research Letters*, *18*(12), 125001. https://doi.org/10.1088/1748-9326/ad0607

Göckede, M., Kwon, M. J., Kittler, F., Heimann, M., Zimov, N., & Zimov, S. (2019). Negative feedback processes following drainage slow down permafrost degradation. *Global Change Biology*, *25*(10), 3254–3266. https://doi.org/10.1111/gcb.14744

Gross, C. D., & Harrison, R. B. (2019). The case for digging deeper: Soil organic carbon storage, dynamics, and controls in our changing world. *Soil Systems*, *3*(2), 28. https://doi.org/10.3390/soilsystems3020028

Haddix, M. L., Gregorich, E. G., Helgason, B. L., Janzen, H., Ellert, B. H., & Francesca Cotrufo, M. (2020). Climate, carbon content, and soil texture control the independent formation and persistence of particulate and mineral-associated organic matter in soil. *Geoderma*, *363*, 114160. https://doi.org/10.1016/j.geoderma.2019.114160

Hayes, D. J., Kicklighter, D. W., McGuire, A. D., Chen, M., Zhuang, Q., Yuan, F., et al. (2014). The impacts of recent permafrost thaw on land–atmosphere greenhouse gas exchange. *Environmental Research Letters*, *9*(4), 045005. https://doi.org/10.1088/1748-9326/9/4/045005

Hayes, D. J., McGuire, A. D., Kicklighter, D. W., Gurney, K. R., Burnside, T. J., & Melillo, J. M. (2011). Is the northern high-latitude land-based CO_2 sink weakening? *Global Biogeochemical Cycles*, *25*(3), GB3018. https://doi.org/10.1029/2010GB003813

Hicks Pries, C. E., Sulman, B. N., West, C., O'Neill, C., Poppleton, E., Porras, R. C., et al. (2018). Root litter decomposition slows with soil depth. *Soil Biology and Biochemistry*, *125*, 103–114. https://doi.org/10.1016/j.soilbio.2018.07.002

Hugelius, G., Strauss, J., Zubrzycki, S., Harden, J. W., Schuur, E. A. G., Ping, C. L., et al. (2014). Estimated stocks of circumpolar permafrost carbon with quantified uncertainty ranges and identified data gaps. *Biogeosciences*, *11*(23), 6573–6593. https://doi.org/10.5194/bg-11-6573-2014

Hungate, B. A., Van Groenigen, K.-J., Six, J., Jastrow, J. D., Luo, Y., De Graaff, M.-A., et al. (2009). Assessing the effect of elevated carbon dioxide on soil carbon: A comparison of four meta-analyses. *Global Change Biology*, *15*(8), 2020–2034. https://doi.org/10.1111/j.1365-2486.2009.01866.x

Jafarov, E., & Schaefer, K. (2016). The importance of a surface organic layer in simulating permafrost thermal and carbon dynamics. *The Cryosphere*, *10*(1), 465–475. https://doi.org/10.5194/tc-10-465-2016

Jiang, M., Medlyn, B. E., Drake, J. E., Duursma, R. A., Anderson, I. C., Barton, C. V. M., et al. (2020). The fate of carbon in a mature forest under carbon dioxide enrichment. *Nature*, *580*(7802), 227–231. https://doi.org/10.1038/s41586-020-2128-9

Jin, Z., Zhuang, Q., He, J.-S., Zhu, X., & Song, W. (2015). Net exchanges of methane and carbon dioxide on the Qinghai-Tibetan Plateau from 1979 to 2100. *Environmental Research Letters*, *10*(8), 16. https://doi.org/10.1088/1748-9326/10/8/085007/pdf

Junttila, S., Kelly, J., Kljun, N., Aurela, M., Klemedtsson, L., Lohila, A., et al. (2021). Upscaling northern peatland CO_2 fluxes using satellite remote sensing data. *Remote Sensing*, *13*(4), 818. https://doi.org/10.3390/rs13040818

Keenan, T. F., Luo, X., Stocker, B. D., De Kauwe, M. G., Medlyn, B. E., Prentice, I. C., et al. (2023). A constraint on historic growth in global photosynthesis due to rising CO_2. *Nature Climate Change*, *13*(12), 1376–1381. https://doi.org/10.1038/s41558-023-01867-2

Kicklighter, D. W., Melillo, J. M., Monier, E., Sokolov, A. P., & Zhuang, Q. (2019). Future nitrogen availability and its effect on carbon sequestration in Northern Eurasia. *Nature Communications*, *10*(1), 3024. https://doi.org/10.1038/s41467-019-10944-0

Kirschbaum, M. U. F., Don, A., Beare, M. H., Hedley, M. J., Pereira, R. C., Curtin, D., et al. (2021). Sequestration of soil carbon by burying it deeper within the profile: A theoretical exploration of three possible mechanisms. *Soil Biology and Biochemistry*, *163*, 108432. https://doi.org/10.1016/j.soilbio.2021.108432

Koven, C. D., Lawrence, D. M., & Riley, W. J. (2015). Permafrost carbon−climate feedback is sensitive to deep soil carbon decomposability but not deep soil nitrogen dynamics. *Proceedings of the National Academy of Sciences*, 201415123.

Koven, C. D., Riley, W. J., Subin, Z. M., Tang, J. Y., Torn, M. S., Collins, W. D., et al. (2013). The effect of vertically resolved soil biogeochemistry and alternate soil C and N models on C dynamics of CLM4. *Biogeosciences*, *10*(11), 7109–7131. https://doi.org/10.5194/bg-10-7109-2013

Lange, S. (2019). Trend-preserving bias adjustment and statistical downscaling with ISIMIP3BASD (v1.0). *Geoscientific Model Development*, *12*(7), 3055–3070. https://doi.org/10.5194/gmd-12-3055-2019

Lehmann, J., Hansel, C. M., Kaiser, C., Kleber, M., Maher, K., Manzoni, S., et al. (2020). Persistence of soil organic carbon caused by functional complexity. *Nature Geoscience*, *13*(8), 529–534. https://doi.org/10.1038/s41561-020-0612-3

Li, F., Yang, G., Peng, Y., Wang, G., Qin, S., Song, Y., et al. (2020). Warming effects on methane fluxes differ between two alpine grasslands with contrasting soil water status. *Agricultural and Forest Meteorology*, *290*, 107988. https://doi.org/10.1016/j.agrformet.2020.107988

Li, J., Yan, D., Pendall, E., Pei, J., Noh, N. J., He, J.-S., et al. (2018). Depth dependence of soil carbon temperature sensitivity across Tibetan permafrost regions. *Soil Biology and Biochemistry*, *126*, 82–90. https://doi.org/10.1016/j.soilbio.2018.08.015

Liu, L., Zhao, D., Wei, J., Zhuang, Q., Gao, X., Zhu, Y., et al. (2021). Permafrost sensitivity to global warming of 1.5°C and 2°C in the Northern Hemisphere. *Environmental Research Letters*, *16*(3), 034038. https://doi.org/10.1088/1748-9326/abd6a8

Liu, L., Zhuang, Q., Zhao, D., Wei, J., & Zheng, D. (2024). The fate of deep permafrost carbon in northern high latitudes in the 21st century: A process-based modeling analysis [Dataset]. *Figshare*. https://doi.org/10.6084/m9.figshare.25705806.v1

Lupascu, M., Welker, J. M., Seibt, U., Maseyk, K., Xu, X., & Czimczik, C. I. (2014). High Arctic wetting reduces permafrost carbon feedbacks to climate warming. *Nature Climate Change*, *4*(1), 51–55. https://doi.org/10.1038/nclimate2058

MacDougall, A. H., & Knutti, R. (2016). Projecting the release of carbon from permafrost soils using a perturbed parameter ensemble modelling approach. *Biogeosciences*, *13*(7), 2123–2136. https://doi.org/10.5194/bg-13-2123-2016

McGuire, A. D., Joyce, L. A., Kicklighter, D. W., Melillo, J. M., Esser, G., & Vorosmarty, C. J. (1993). Productivity response of climax temperate forests to elevated temperature and carbon dioxide: A North American comparison between two global models. *Climatic Change*, *24*(4), 287–310. https://doi.org/10.1007/BF01091852

McGuire, A. D., Koven, C., Lawrence, D. M., Clein, J. S., Xia, J. Y., Beer, C., et al. (2016). Variability in the sensitivity among model simulations of permafrost and carbon dynamics in the permafrost region between 1960 and 2009. *Global Biogeochemical Cycles*, *30*(7), 1015–1037. https://doi.org/10.1002/2016gb005405

McGuire, A. D., Lawrence, D. M., Koven, C., Clein, J. S., Burke, E., Chen, G. S., et al. (2018). Dependence of the evolution of carbon dynamics in the northern permafrost region on the trajectory of climate change. *Proceedings of the National Academy of Sciences of the United States of America*, *115*(15), 3882–3887. https://doi.org/10.1073/pnas.1719903115

McGuire, A. D., Melillo, J. M., Joyce, L. A., Kicklighter, D. W., Grace, A. L., Moore, B., & Vorosmarty, C. J. (1992). Interactions between carbon and nitrogen dynamics in estimating net primary productivity for potential vegetation in North America. *Global Biogeochemical Cycles*, *6*(2), 101–124. https://doi.org/10.1029/92GB00219

Meredith, M. P., Sommerkorn, M., Cassotta, S., Derksen, C., Ekaykin, A. A., Hollowed, A. B., et al. (2019). Chapter 3: Polar regions. In *The Ocean and Cryosphere in a Changing Climate: Summary for Policymakers* (pp. 3-1–3-173). Intergovernmental Panel on Climate Change. Retrieved from https://research.monash.edu/en/publications/chapter-3-polar-regions

Miner, K. R., Turetsky, M. R., Malina, E., Bartsch, A., Tamminen, J., McGuire, A. D., et al. (2022). Permafrost carbon emissions in a changing Arctic. *Nature Reviews Earth & Environment*, *3*(1), 55–67. https://doi.org/10.1038/s43017-021-00230-3

Mishra, U., Hugelius, G., Shelef, E., Yang, Y., Strauss, J., Lupachev, A., et al. (2021). Spatial heterogeneity and environmental predictors of permafrost region soil organic carbon stocks. *Science Advances*, *7*(9), eaaz5236. https://doi.org/10.1126/sciadv.aaz5236

Monteux, S., Keuper, F., Fontaine, S., Gavazov, K., Hallin, S., Juhanson, J., et al. (2020). Carbon and nitrogen cycling in Yedoma permafrost controlled by microbial functional limitations. *Nature Geoscience*, *13*(12), 794–798. https://doi.org/10.1038/s41561-020-00662-4

Moss, R. H., Edmonds, J. A., Hibbard, K. A., Manning, M. R., Rose, S. K., van Vuuren, D. P., et al. (2010). The next generation of scenarios for climate change research and assessment. *Nature*, *463*(7282), 747–756. https://doi.org/10.1038/nature08823

Moyano, F. E., Manzoni, S., & Chenu, C. (2013). Responses of soil heterotrophic respiration to moisture availability: An exploration of processes and models. *Soil Biology and Biochemistry*, *59*, 72–85. https://doi.org/10.1016/j.soilbio.2013.01.002

Natali, S. M., Bronen, R., Cochran, P., Holdren, J. P., Rogers, B. M., & Treharne, R. (2022). Incorporating permafrost into climate mitigation and adaptation policy. *Environmental Research Letters*, *17*(9), 091001. https://doi.org/10.1088/1748-9326/ac8c5a

Neigh, C. S. R., Nelson, R. F., Ranson, K. J., Margolis, H. A., Montesano, P. M., Sun, G., et al. (2013). Taking stock of circumboreal forest carbon with ground measurements, airborne and spaceborne LiDAR. *Remote Sensing of Environment*, *137*, 274–287. https://doi.org/10.1016/j.rse.2013.06.019

Ni, J., Wu, T., Zhu, X., Hu, G., Zou, D., Wu, X., et al. (2021). Simulation of the present and future projection of permafrost on the Qinghai-Tibet Plateau with statistical and machine learning models. *Journal of Geophysical Research: Atmospheres*, *126*(2), e2020JD033402. https://doi.org/10.1029/2020JD033402

Niu, Z., He, H., Peng, S., Ren, X., Zhang, L., Gu, F., et al. (2021). A process-based model integrating remote sensing data for evaluating ecosystem services. *Journal of Advances in Modeling Earth Systems*, *13*(6), e2020MS002451. https://doi.org/10.1029/2020MS002451

Obu, J., Westermann, S., Bartsch, A., Berdnikov, N., Christiansen, H. H., Dashtseren, A., et al. (2019). Northern Hemisphere permafrost map based on TTOP modelling for 2000–2016 at 1 km^2 scale. *Earth-Science Reviews*, *193*, 299–316. https://doi.org/10.1016/j.earscirev.2019.04.023

O'Neill, B. C., Kriegler, E., Ebi, K. L., Kemp-Benedict, E., Riahi, K., Rothman, D. S., et al. (2017). The roads ahead: Narratives for shared socioeconomic pathways describing world futures in the 21st century. *Global Environmental Change*, *42*, 169–180. https://doi.org/10.1016/j.gloenvcha.2015.01.004

Palmtag, J., Obu, J., Kuhry, P., Richter, A., Siewert, M. B., Weiss, N., et al. (2022). A high spatial resolution soil carbon and nitrogen dataset for the northern permafrost region based on circumpolar land cover upscaling. *Earth System Science Data*, *14*(9), 4095–4110. https://doi.org/10.5194/essd-14-4095-2022

Pastore, M. A., Hobbie, S. E., & Reich, P. B. (2021). Sensitivity of grassland carbon pools to plant diversity, elevated CO_2, and soil nitrogen addition over 19 years. *Proceedings of the National Academy of Sciences*, *118*(17), e2016965118. https://doi.org/10.1073/pnas.2016965118

Pastorello, G., Trotta, C., Canfora, E., Chu, H., Christianson, D., Cheah, Y.-W., et al. (2020). The FLUXNET2015 dataset and the ONEFlux processing pipeline for eddy covariance data. *Scientific Data*, *7*(1), 225. https://doi.org/10.1038/s41597-020-0534-3

Pegoraro, E. F., Mauritz, M. E., Ogle, K., Ebert, C. H., & Schuur, E. A. G. (2021). Lower soil moisture and deep soil temperatures in thermokarst features increase old soil carbon loss after 10 years of experimental permafrost warming. *Global Change Biology*, *27*(6), 1293–1308. https://doi.org/10.1111/gcb.15481

Ping, C. L., Jastrow, J. D., Jorgenson, M. T., Michaelson, G. J., & Shur, Y. L. (2015). Permafrost soils and carbon cycling. *Soil*, *1*(1), 147–171. https://doi.org/10.5194/soil-1-147-2015

Raich, J. W., Rastetter, E. B., Melillo, J. M., Kicklighter, D. W., Steudler, P. A., Peterson, B. J., et al. (1991). Potential net primary productivity in South America: Application of a global model. *Ecological Applications*, *1*(4), 399–429. https://doi.org/10.2307/1941899

Ramm, E., Liu, C., Ambus, P., Butterbach-Bahl, K., Hu, B., Martikainen, P. J., et al. (2022). A review of the importance of mineral nitrogen cycling in the plant-soil-microbe system of permafrost-affected soils—Changing the paradigm. *Environmental Research Letters*, *17*(1), 013004. https://doi.org/10.1088/1748-9326/ac417e

Raynolds, M. K., Walker, D. A., Epstein, H. E., Pinzon, J. E., & Tucker, C. J. (2012). A new estimate of tundra-biome phytomass from trans-Arctic field data and AVHRR NDVI. *Remote Sensing Letters*, *3*(5), 403–411. https://doi.org/10.1080/01431161.2011.609188

Rodenhizer, H., Ledman, J., Mauritz, M., Natali, S. M., Pegoraro, E., Plaza, C., et al. (2020). Carbon thaw rate doubles when accounting for subsidence in a permafrost warming experiment. *Journal of Geophysical Research: Biogeosciences*, *125*(6), e2019JG005528. https://doi.org/10.1029/2019JG005528

Rumpel, C., & Kögel-Knabner, I. (2011). Deep soil organic matter—A key but poorly understood component of terrestrial C cycle. *Plant and Soil*, *338*(1), 143–158. https://doi.org/10.1007/s11104-010-0391-5

Schädel, C., Rogers, B. M., Lawrence, D. M., Koven, C. D., Brovkin, V., Burke, E. J., et al. (2024). Earth system models must include permafrost carbon processes. *Nature Climate Change*, *14*(2), 114–116. https://doi.org/10.1038/s41558-023-01909-9

Schädel, C., Schuur, E. A. G., Bracho, R., Elberling, B., Knoblauch, C., Lee, H., et al. (2014). Circumpolar assessment of permafrost C quality and its vulnerability over time using long-term incubation data. *Global Change Biology*, *20*(2), 641–652. https://doi.org/10.1111/gcb.12417

Schneider von Deimling, T., Grosse, G., Strauss, J., Schirrmeister, L., Morgenstern, A., Schaphoff, S., et al. (2015). Observation-based modelling of permafrost carbon fluxes with accounting for deep carbon deposits and thermokarst activity. *Biogeosciences*, *12*(11), 3469–3488. https://doi.org/10.5194/bg-12-3469-2015

Schuur, E. A. G., Abbott, B. W., Commane, R., Ernakovich, J., Euskirchen, E., Hugelius, G., et al. (2022). Permafrost and climate change: Carbon cycle feedbacks from the warming Arctic. *Annual Review of Environment and Resources*, *47*(1), 343–371. https://doi.org/10.1146/annurev-environ-012220-011847

Schuur, E. A. G., Bockheim, J., Canadell, J. G., Euskirchen, E., Field, C. B., Goryachkin, S. V., et al. (2008). Vulnerability of permafrost carbon to climate change: Implications for the global carbon cycle. *BioScience*, *58*(8), 701–714. https://doi.org/10.1641/B580807

Schuur, E. A. G., McGuire, A. D., Schadel, C., Grosse, G., Harden, J. W., Hayes, D. J., et al. (2015). Climate change and the permafrost carbon feedback. *Nature*, *520*(7546), 171–179. https://doi.org/10.1038/nature14338

Shu, S., Jain, A. K., Koven, C. D., & Mishra, U. (2020). Estimation of permafrost SOC stock and turnover time using a land surface model with vertical heterogeneity of permafrost soils. *Global Biogeochemical Cycles*, *34*(11), e2020GB006585. https://doi.org/10.1029/2020gb006585

Sigurdsson, B. D., Medhurst, J. L., Wallin, G., Eggertsson, O., & Linder, S. (2013). Growth of mature boreal Norway spruce was not affected by elevated [CO(2)] and/or air temperature unless nutrient availability was improved. *Tree Physiology*, *33*(11), 1192–1205. https://doi.org/10.1093/treephys/tpt043

Slater, A. G., & Lawrence, D. M. (2013). Diagnosing present and future permafrost from climate models. *Journal of Climate*, *26*(15), 5608–5623. https://doi.org/10.1175/jcli-d-12-00341.1

Song, X., Wang, G., Ran, F., Huang, K., Sun, J., & Song, C. (2020). Soil moisture as a key factor in carbon release from thawing permafrost in a boreal forest. *Geoderma*, *357*, 113975. https://doi.org/10.1016/j.geoderma.2019.113975

Stepanenko, V. M., Repina, I. A., Fedosov, V. E., Zilitinkevich, S. S., & Lykossov, V. N. (2020). An overview of parameterezations of heat transfer over moss-covered surfaces in the Earth system models. *Izvestiya, Atmospheric and Oceanic Physics*, *56*(2), 101–111. https://doi.org/10.1134/S0001433820020139

Takaku, J., Tadono, T., Doutsu, M., Ohgushi, F., & Kai, H. (2020). Updates of 'AW3D30' ALOS global digital surface model with other open access datasets. *The International Archives of the Photogrammetry, Remote Sensing and Spatial Information Sciences*, *43*, 183–189. https://doi.org/10.5194/isprs-archives-xliii-b4-2020-183-2020

Tao, J., Riley, W. J., & Zhu, Q. (2024). Evaluating the impact of peat soils and snow schemes on simulated active layer thickness at pan-Arctic permafrost sites. *Environmental Research Letters*, *19*(5), 054027. https://doi.org/10.1088/1748-9326/ad38ce

Tebaldi, C., Debeire, K., Eyring, V., Fischer, E., Fyfe, J., Friedlingstein, P., et al. (2021). Climate model projections from the Scenario Model Intercomparison Project (ScenarioMIP) of CMIP6. *Earth System Dynamics*, *12*(1), 253–293. https://doi.org/10.5194/esd-12-253-2021

Terrer, C., Jackson, R. B., Prentice, I. C., Keenan, T. F., Kaiser, C., Vicca, S., et al. (2019). Nitrogen and phosphorus constrain the CO_2 fertilization of global plant biomass. *Nature Climate Change*, *9*(9), 684–689. https://doi.org/10.1038/s41558-019-0545-2

Terrer, C., Phillips, R. P., Hungate, B. A., Rosende, J., Pett-Ridge, J., Craig, M. E., et al. (2021). A trade-off between plant and soil carbon storage under elevated CO_2. *Nature*, *591*(7851), 599–603. https://doi.org/10.1038/s41586-021-03306-8

Tian, H., Melillo, J. M., Kicklighter, D. W., McGuire, A. D., & Helfrich, J. (1999). The sensitivity of terrestrial carbon storage to historical climate variability and atmospheric CO_2 in the United States. *Tellus B: Chemical and Physical Meteorology*, *51*(2), 414–452. https://doi.org/10.3402/tellusb.v51i2.16318

Treat, C. C., Virkkala, A.-M., Burke, E., Bruhwiler, L., Chatterjee, A., Fisher, J. B., et al. (2024). Permafrost carbon: Progress on understanding stocks and fluxes across northern terrestrial ecosystems. *Journal of Geophysical Research: Biogeosciences*, *129*(3), e2023JG007638. https://doi.org/10.1029/2023JG007638

Turetsky, M. R., Abbott, B. W., Jones, M. C., Anthony, K. W., Olefeldt, D., Schuur, E. A. G., et al. (2020). Carbon release through abrupt permafrost thaw. *Nature Geoscience*, *13*(2), 138–143. https://doi.org/10.1038/s41561-019-0526-0

van Groenigen, K. J., Qi, X., Osenberg, C. W., Luo, Y., & Hungate, B. A. (2014). Faster decomposition under increased atmospheric CO_2 limits soil carbon storage. *Science*, *344*(6183), 508–509. https://doi.org/10.1126/science.1249534

Varney, R. M., Chadburn, S. E., Burke, E. J., & Cox, P. M. (2022). Evaluation of soil carbon simulation in CMIP6 Earth system models. *Biogeosciences*, *19*(19), 4671–4704. https://doi.org/10.5194/bg-19-4671-2022

Virkkala, A.-M., Aalto, J., Rogers, B. M., Tagesson, T., Treat, C. C., Natali, S. M., et al. (2021). Statistical upscaling of ecosystem CO_2 fluxes across the terrestrial tundra and boreal domain: Regional patterns and uncertainties. *Global Change Biology*, *27*(17), 4040–4059. https://doi.org/10.1111/gcb.15659

Walker, A. P., De Kauwe, M. G., Bastos, A., Belmecheri, S., Georgiou, K., Keeling, R. F., et al. (2021). Integrating the evidence for a terrestrial carbon sink caused by increasing atmospheric CO_2. *New Phytologist*, *229*(5), 2413–2445. https://doi.org/10.1111/nph.16866

Walker, A. P., De Kauwe, M. G., Medlyn, B. E., Zaehle, S., Iversen, C. M., Asao, S., et al. (2019). Decadal biomass increment in early secondary succession woody ecosystems is increased by CO_2 enrichment. *Nature Communications*, *10*(1), 454. https://doi.org/10.1038/s41467-019-08348-1

Wang, T., Yang, D., Yang, Y., Piao, S., Li, X., Cheng, G., & Fu, B. (2020). Permafrost thawing puts the frozen carbon at risk over the Tibetan Plateau. *Science Advances*, *6*(19), eaaz3513. https://doi.org/10.1126/sciadv.aaz3513

Welter, D. E., White, J. T., Hunt, R. J., & Doherty, J. E. (2015). Approaches in highly parameterized inversion—PEST++ Version 3, a Parameter ESTimation and uncertainty analysis software suite optimized for large environmental models (7-C12). Retrieved from https://pubs.usgs.gov/publication/tm7C12

Witzgall, K., Vidal, A., Schubert, D. I., Höschen, C., Schweizer, S. A., Buegger, F., et al. (2021). Particulate organic matter as a functional soil component for persistent soil organic carbon. *Nature Communications*, *12*(1), 4115. https://doi.org/10.1038/s41467-021-24192-8

Wu, C., Yeh, P. J.-F., Ju, J., Chen, Y.-Y., Xu, K., Dai, H., et al. (2021). Assessing the spatiotemporal uncertainties in future meteorological droughts from CMIP5 models, emission scenarios, and bias corrections. *Journal of Climate*, *34*(5), 1903–1922. https://doi.org/10.1175/JCLI-D-20-0411.1

Wu, X., Nan, Z., Zhao, S., Zhao, L., & Cheng, G. (2018). Spatial modeling of permafrost distribution and properties on the Qinghai-Tibet Plateau. *Permafrost and Periglacial Processes*, *29*(2), 86–99. https://doi.org/10.1002/ppp.1971

Wu, Y., Miao, C., Fan, X., Gou, J., Zhang, Q., & Zheng, H. (2022). Quantifying the uncertainty sources of future climate projections and narrowing uncertainties with bias correction techniques. *Earth's Future*, *10*(11), e2022EF002963. https://doi.org/10.1029/2022EF002963

Yang, Y. H., Fang, J. Y., Ji, C. J., & Han, W. X. (2009). Above- and belowground biomass allocation in Tibetan grasslands. *Journal of Vegetation Science*, *20*(1), 177–184. https://doi.org/10.1111/j.1654-1103.2009.05566.x

Yao, Y., Ciais, P., Viovy, N., Li, W., Cresto-Aleina, F., Yang, H., et al. (2021). A data-driven global soil heterotrophic respiration dataset and the drivers of its inter-annual variability. *Global Biogeochemical Cycles*, *35*(8), e2020GB006918. https://doi.org/10.1029/2020GB006918

Yokohata, T., Saito, K., Takata, K., Nitta, T., Satoh, Y., Hajima, T., et al. (2020). Model improvement and future projection of permafrost processes in a global land surface model. *Progress in Earth and Planetary Science*, *7*(1), 69. https://doi.org/10.1186/s40645-020-00380-w

Yun, H., Zhu, Q., Tang, J., Zhang, W., Chen, D., Ciais, P., et al. (2023). Warming, permafrost thaw and increased nitrogen availability as drivers for plant composition and growth across the Tibetan Plateau. *Soil Biology and Biochemistry*, *182*, 109041. https://doi.org/10.1016/j.soilbio.2023.109041

Zaehle, S., Medlyn, B. E., De Kauwe, M. G., Walker, A. P., Dietze, M. C., Hickler, T., et al. (2014). Evaluation of 11 terrestrial carbon–nitrogen cycle models against observations from two temperate Free-Air CO_2 Enrichment studies. *New Phytologist*, *202*(3), 803–822. https://doi.org/10.1111/nph.12697

Zhu, Q., & Zhuang, Q. (2014). Parameterization and sensitivity analysis of a process-based terrestrial ecosystem model using adjoint method. *Journal of Advances in Modeling Earth Systems*, *6*(2), 315–331. https://doi.org/10.1002/2013MS000241

Zhuang, Q., He, J., Lu, Y., Ji, L., Xiao, J., & Luo, T. (2010). Carbon dynamics of terrestrial ecosystems on the Tibetan Plateau during the 20th century: An analysis with a process-based biogeochemical model. *Global Ecology and Biogeography*, *19*(5), 649–662. https://doi.org/10.1111/j.1466-8238.2010.00559.x

Zhuang, Q., McGuire, A. D., Melillo, J. M., Clein, J. S., Dargaville, R. J., Kicklighter, D. W., et al. (2011). Carbon cycling in extratropical terrestrial ecosystems of the Northern Hemisphere during the 20th century: A modeling analysis of the influences of soil thermal dynamics. *Tellus B: Chemical and Physical Meteorology*, *55*(3), 751–776. https://doi.org/10.3402/tellusb.v55i3.16368

Zhuang, Q., Romanovsky, V. E., & McGuire, A. D. (2001). Incorporation of a permafrost model into a large-scale ecosystem model: Evaluation of temporal and spatial scaling issues in simulating soil thermal dynamics. *Journal of Geophysical Research*, *106*(D24), 33649–33670. https://doi.org/10.1029/2001JD900151

References From the Supporting Information

Jin, Z., Zhuang, Q., He, J.-S., Luo, T., & Shi, Y. (2013). Phenology shift from 1989 to 2008 on the Tibetan Plateau: An analysis with a process-based soil physical model and remote sensing data. *Climatic Change*, *119*(2), 435–449. https://doi.org/10.1007/s10584-013-0722-7

McGuire, A. D., Melillo, J. M., Kicklighter, D. W., Pan, Y., Xiao, X., Helfrich, J., et al. (1997). Equilibrium responses of global net primary production and carbon storage to doubled atmospheric carbon dioxide: Sensitivity to changes in vegetation nitrogen concentration. *Global Biogeochemical Cycles*, *11*(2), 173–189. https://doi.org/10.1029/97GB00059

Pan, Y., Melillo, J. M., McGuire, A. D., Kicklighter, D. W., Pitelka, L. F., Hibbard, K., et al. (1998). Modeled responses of terrestrial ecosystems to elevated atmospheric CO_2: A comparison of simulations by the biogeochemistry models of the Vegetation/Ecosystem Modeling and Analysis Project (VEMAP). *Oecologia*, *114*(3), 389–404. https://doi.org/10.1007/s004420050462

Zhuang, Q., McGuire, A. D., O'Neill, K. P., Harden, J. W., Romanovsky, V. E., & Yarie, J. (2002). Modeling soil thermal and carbon dynamics of a fire chronosequence in interior Alaska. *Journal of Geophysical Research*, *108*(D1). FFR 3-1–FFR 3-26. https://doi.org/10.1029/2001jd001244